CADMIUM SULFIDE - COPPER SULFIDE

HETEROJUNCTION CELL RESEARCH

Quarterly Progress Report -3

March 1, 1979 to June 1, 1979

XR-9-8063-1 -03

August 1979

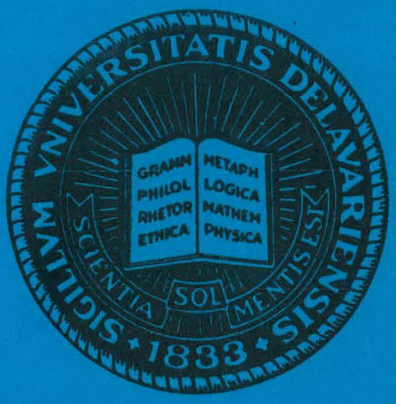

INSTITUTE OF ENERGY CONVERSION
UNIVERSITY OF DELAWARE
NEWARK, DELAWARE 19711

Supported by the Solar Energy Research Institute, Report XR-9-8063-1-03

DISCLAIMER

1. ABSTRACT

Progress has been made on improving the photon efficiency of the planar CdS/Cu_2S solar cell. Currents in excess of 20 mA/cm^2 have been achieved. Mixed sulfide solar cells responsive to heat treatment are now being produced. The morphology of the Cu_2S/CdZnS junction has been examined and found to be significantly different than the morphology on CdS/Cu_2S cells. Efficiencies measured under ELH simulation approaching 8% have been achieved. Work in the analytical task has focused on establishing the experimental techniques to study the trap levels in the CdS and to provide a working model for the voltage instabilities in some (CdZn)S/Cu_2S cells. Cells under roof top exposure continue to be monitored.

2. TABLE OF CONTENTS

APPENDIX

LIST OF ILLUSTRATIONS

3. INTRODUCTION

Improved control on the deposition of CuCl and a modified pre-treatment for the CdS layer have resulted in better current with the planar junction. The variability in CdS substrate material has been progressively reduced during the CdS solar cell program and further improvement has been achieved this quarter.

By using the information developed in Task 1 to direct the mixed sulfide cell program, it has been possible to systematically improve the performance of (CdZn)S/Cu_2S cells. During this month modifications to the mixed sulfide deposition procedure and post deposition heat treatments to reduce the substrate resistivity have resulted in substantial improvements in cell performance. Of equal significance is the fact that cells produced are now responding to the reducing heat treatments developed in Task 1.

A major expansion in scope and reduction in turn around time has been achieved for the routine analysis and feedback aspects of the analysis task. Techniques are being established and the analyses developed for identifying the trap levels in the CdS. A theoretical model has been developed to explain the time dependent open circuit voltage of mixed sulfide cells and this model will guide the experimental effort to eliminate the phenomenum.

Monitoring of cells exposed on the roof continues. Another cell has been sealed between a glass plate and a Kovar sheet and put on test.

4.1 Task 1 Development of CdS/Cu_2S Solar Cells

The need to develop effective light trapping as well as reducing first surface reflection losses has significantly extended the effort on Phase 2 of this task. Progress has however been made in both the development of a good analytical model and in the realization of effective cell structures.

4.1.1 Phase 1 Planar Junction with Good Open Circuit Voltage and Fill Factor

Some difficulty has arisen with excessively high series resistances in planar junction CdS/Cu_2S cells. In order to achieve over 70% fill factor the series resistance of a 1 cm^2 cell must be $\leq 3\ \Omega$. Measurements on parallel solution-reaction cells proves that the cause is not related to the CdS substrate and electrolytic analysis of the Cu_2S layer indicates that the desired thicknesses are being achieved. A thorough review of the solid state reaction procedure and detailed analysis of the Cu_2S layer was carried out. As a result much better Cu_2S layers are now being produced with better reproducibility.

4.2.2 Phase 2 Achievement of Low Photon Losses

As described at the SERI Semi-Annual review meeting the necessity of achieving light trapping has significantly extended this phase. A model has now been developed to permit an analytical attack on the problem. The model is fully described in the appended paper which was presented at the Berlin Photovoltaic meeting.

4.1.3 Phase 3 Combine Technologies to Give $J_{sc} > 27\ mA/cm^2$

Substantial difficulties in achieving the goal of this phase have been caused by the substrate to substrate variation of CdS properties.

A procedure to rapidly test the CdS by making a standard textured cell is being developed.

A light HCl etch (20% HCl at 60°C) to remove 0.5 μm of CdS has proved beneficial in both voltage and current for the planar cells resulting in the highest light generated currents that have been achieved for this structure. Cell 20858.123 gave 20.8 mA/cm^2 and 21.5 mA/cm^2 before and after deposition of TiO_x/SiO_2 anti-reflection coating, under 100 mW/cm^2 solar simulation.

4.2 Task 2 Development of (CdZn)S/Cu_2S Solar Cells

The specific phases of Task 2 addressed during the past quarter were the optimization of (CdZn)S films and the investigation of the process of junction formation. Thin film optimization requires the achievement of not only the appropriate resistivity (ρ < 20 ohm-cm) and thickness (t > 20 μm), but also the attainment of the appropriate film microstructure. The formation of the junction was monitored by the analysis of I-V curves and photocapacitance data from cells subjected to a sequence of heat treatments.

4.2.1 Phase 1 Optimum (CdZn)S Films

The preparation of 20-30 μm thick (CdZn)S films having zinc composition in the range of 10-20% with resistivities values less than ∿ 20 ohm-cm, can be reproducibly realized. Using the concentric source design,[1] films exhibiting these properties, and which are compositionally homogeneous over an eight centimeter square substrate, are routinely prepared. Typically, these films have been grown at deposition rates of less than 1.5 μm/min on zinc plated copper substrates held at 200°C.

4.2.2 Phase 2 Develop Junction Morphology

The design strategy for fabricating the other components of a (CdZn)S based solar cell was the same as the cell design which led to the outdoor conversion efficiencies of 9.15%[2] in the CdS/Cu_2S system. Specifically, the (CdZn)S surface was first textured, (using a 50% HCl etch at 60°C for 1 second) and then the heterojunction layer of Cu_2S was formed by the immersion of the (CdZn)S film in a solution of CuCl. Contrary to early findings on (CdZn)S

films prepared from multiple sources,[3] the rate of Cu_2S formation did not depend markedly on the zinc content of the (CdZn)S film. Figure 1 shows a plot of the equivalent thickness of copper sulfide, measured by the electrochemical method,[4] as a function of reaction time for the indicated parametric set of zinc compositions. A Cu_2S formation time was selected to achieve an equivalent Cu_2S thickness of 0.3 μm. The device fabrication was completed by the application of an 80 line/inch gold grid prepared by vacuum evaporation through an aperture mask. The best such (CdZn)S/Cu_2S cell had an open circuit voltage of 599 mV, short circuit current of 15.8 mA/cm^2, and a fill factor of 65.2% under ELH simulation of 83 mW/cm^2 equivalent power. The (CdZn)S substrate contained 19% zinc and had a resistivity of 21 Ω-cm.

Optical cross-sections of devices prepared as above indicated the presence of 4-6 μm long Cu_2S intrusions into the CdS. These intrusions were observed with much higher resolution by the careful removal of the (CdZn)S layer from a (CdZn)S/Cu_2S junction. The SEM micrographs of the free standing Cu_2S revealed the existence of 6-8 μm long cone-like Cu_2S structures (i.e. "intruding" into the (CdZn)S). Cu_2S intrusions are also present at CdS/Cu_2S junctions, however, they appear as "walls" around the CdS columnar boundaries, and typically extend only 1-2 μm into the CdS. Figure 2 shows representative areas of these two types. These intrusions are expected to strongly influence the solar cell device characteristics, and the V_{oc} value of devices exhibiting long cone like intrusions is found to decrease when the device is held in the open circuit condition. The formation of these intrusions is expected to depend on the (CdZn)S microstructure, and will be influenced by the manner in which the Cu_2S is formed.

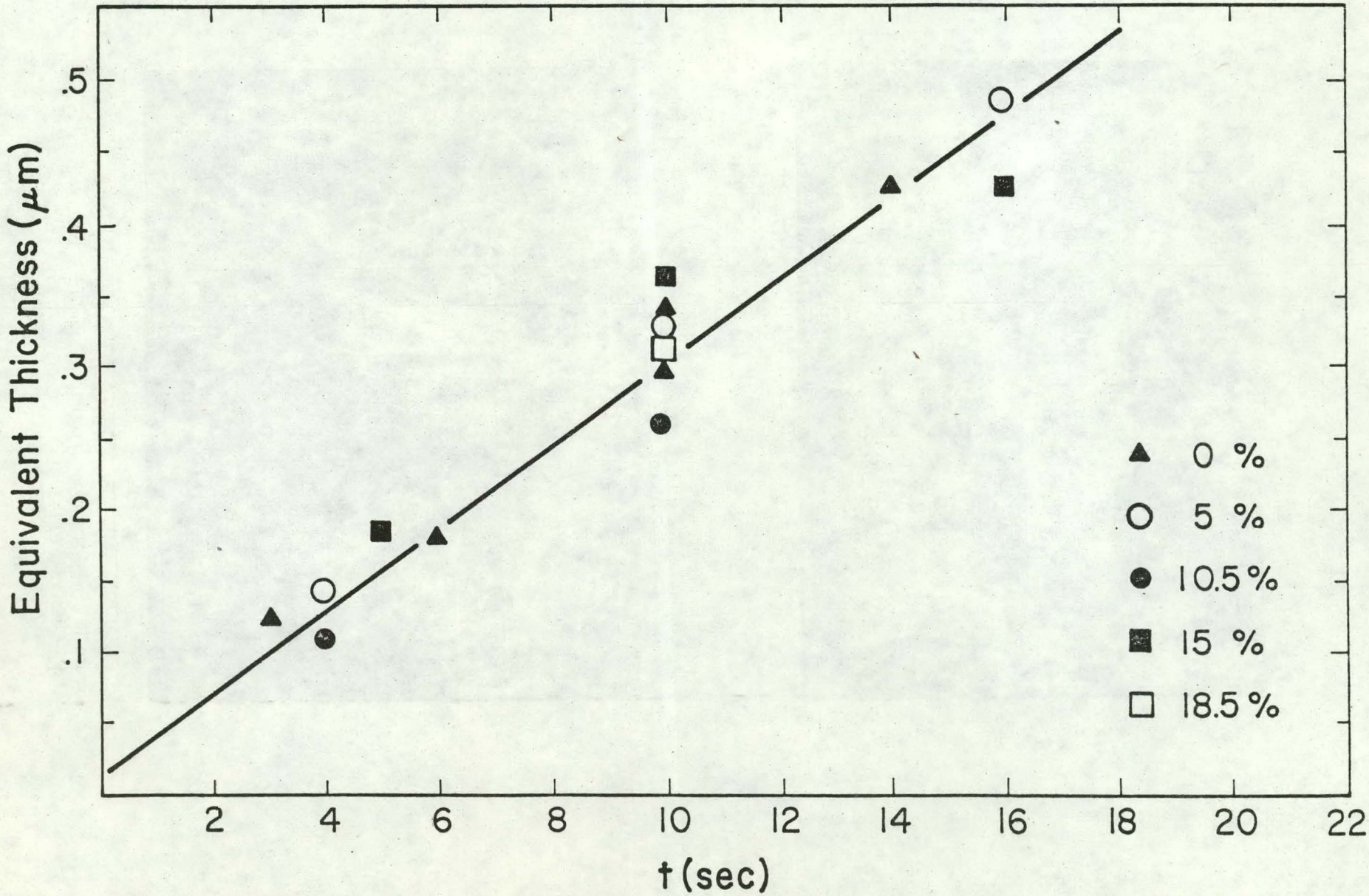

Fig. 1 Formation rate of Cu_2S by solution reaction for (CdZn)S films of various zinc composition.

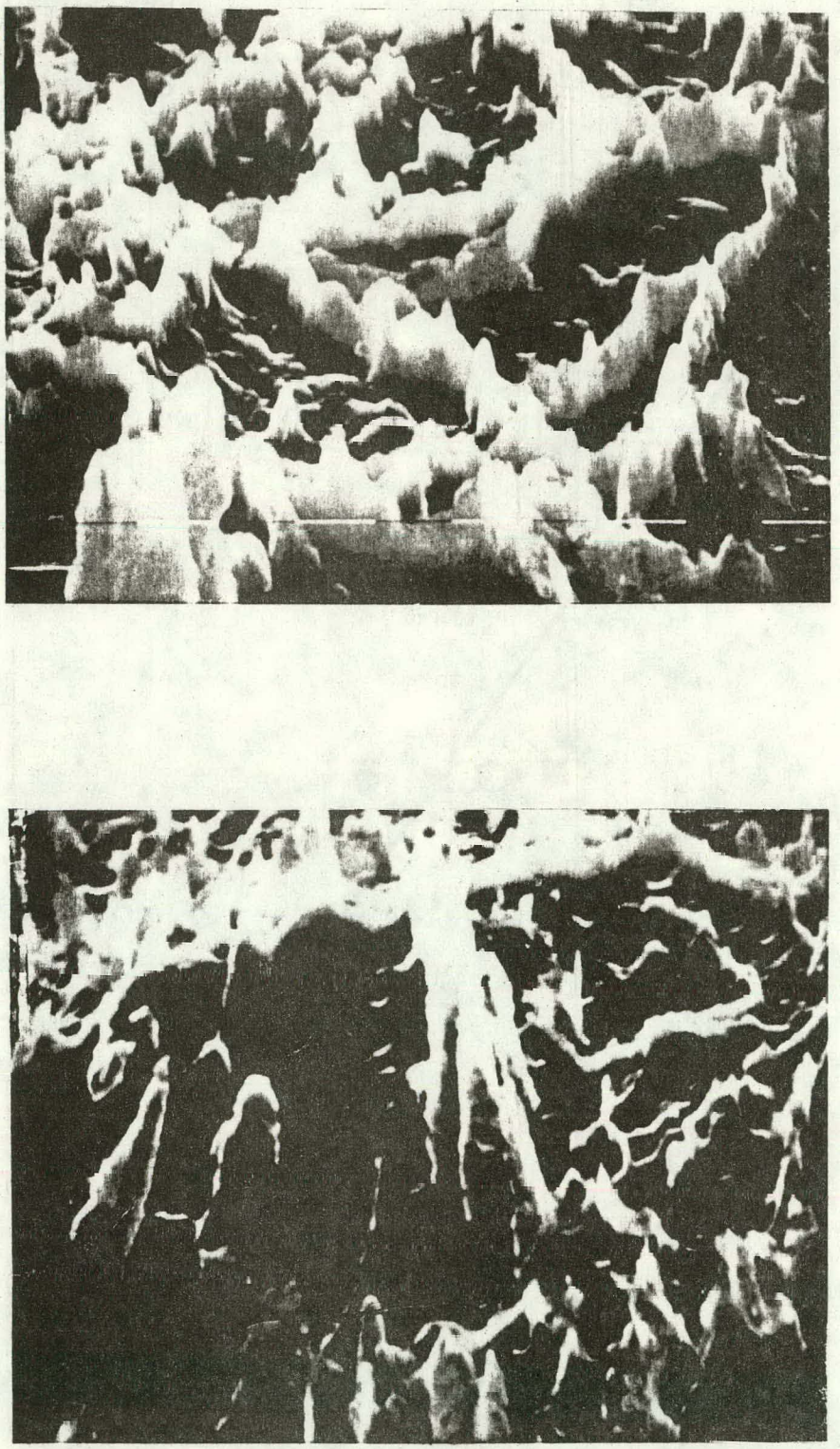

Fig. 2 Scanning Electron Micrographs of Cu_2S removed from CdS and (CdZn)S cells.

a) CdS cell 778.B14
b) (CdZn)S cell M154.B11 (19% Zn)

Both micrographs x 10,000

Although the present cell performance has greatly improved over the former results,[5] the best short circuit current is still about 5 mA/cm^2 less than the best short circuit current measured under the IEC simulator for a CdS/Cu_2S cell of the same design. In addition the fill factor for the (CdZn)S/Cu_2S cells is typically 10-15% less than achieved with CdS/Cu_2S. The heat treatment of the (CdZn)S cells has not improved performance, but rather has resulted in a general degradation of cell properties in marked contrast to the behavior with CdS/Cu_2S.

Preliminary microstructure analysis of the (CdZn)S indicates that the number of subgrains per unit area can be decreased by increasing the film growth rate. It is planned to utilize this change in growth conditions in order to reduce the frequency of Cu_2S intrusions. Higher growth rates will also yield films having lower electrical resistivity which should reduce fill factor losses due to series resistance, and also allow for a more favorable collection field[6] in the (CdZn)S at the junction leading to increased short circuit currents.

The first cells have been prepared on a (CdZn)S film grown at a higher than usual rate of 2.5 μm/min. The best cell had an open circuit voltage of 579 mV, a short circuit current of 15.6 mA/cm^2, (no anti-reflection coating) and a fill factor of 71.2% under the IEC solar simulator at 83 mW/cm^2 equivalent power. The (CdZn)S resistivity was 15 Ω-cm and the Zn content was 14%. Of particular significance is the fact that it was possible to improve the properties of this set of cells by heat treatments. Specifically, a 16 hour heat treatment at 170°C in carbon monoxide optimized the above cell.

4.3 Task 3 Electro-Optical Analysis

4.3.1 Phase 1 Feedback Analysis

In order to improve and automate existing test facilities some form of software development was needed for the microcomputer processors which were built into the test systems. A Digital Equipment Corporation floppy disc based IIVO3 system was acquired and high speed communication lines were established between it and the remote processors. This allows software to be rapidly developed, documented, and loaded into the proper test system. With this capability one can easily create new testing protocols or modify existing ones. It also allows more complex programs to be written, which leads to more automation of the test procedure, and more real time results available to the operating technician. The system was installed during this quarter, and programs for the solar simulator I-V tester were developed. The first set of programs automatically samples the current waveform as a test is performed, and extracts V_{oc}, J_{sc}, V_{mp}, J_{mp}. It then calculates the component values for a lumped equivalent circuit and prints R_s, G_{sh}, J_L and J_o. Software has also been written to operate the microprocessor controlled spectral response test facility. It is now in the process of being debugged.

The new test capabilities are being developed. A facility to allow rooftop solar cell life studies has been designed, and a prototype has been constructed and tested. It allows remote testing of arrays, cells within arrays, and single cells to track degradation in cell performance. The system as designed can select one of 1000 cells, and can be expanded. Cells are selected by thumbwheel switches which are read by CMOS digital logic. The logic controls relays which connect the proper cell to a data bus. The

data bus is connected to an indoor cell I-V tester. The system is designed to be easily automated. Also monitored at the cell location is temperature and solar insolation.

The second new test facility is a Laser Spot Scanner similar to one developed by D. Sawyer of NBS. It will allow rapid scanning of cells to detect spatial inhomogeneity in cell response. This will be used to screen cell material in the early stages of cell production. The system has been designed and ordered, and components are beginning to arrive.

The I-V cell Tester and Spectral Response System will become more automated with work beginning on the design of a centralized data base. The Rooftop Life Test Facility will be installed and optimized. Construction on the Laser Scanner will continue and should become operational next quarter.

4.3.2 Phase 2 and 3 Map Junction Field CdS and (CdZn)S

The break in 1/C versus η_c-1 curves which was seen at high intensity was found to be an instrumental problem related to the silicon solar cell which was being used as a reference cell. Recent measurements confirm the previous results obtained using the spectral response apparatus. Fig. 3 shows the results on cell 675A1-2. The linear region extends from 0.03 to 1.25 AM1 and yields $S_I/\mu = 3.1 \times 10^3 V/cm$, $\eta_Q = 0.47$.

4.3.3 Phase 4 Quantify Interface Recombination

The voltage dependent J_L measurements were extended to include intensity variation of the filtered bias light. A summary of the results are contained in a paper presented by L. Kilgren at the Photovoltaic Solar Energy Conference in Berlin. (Appendix B).

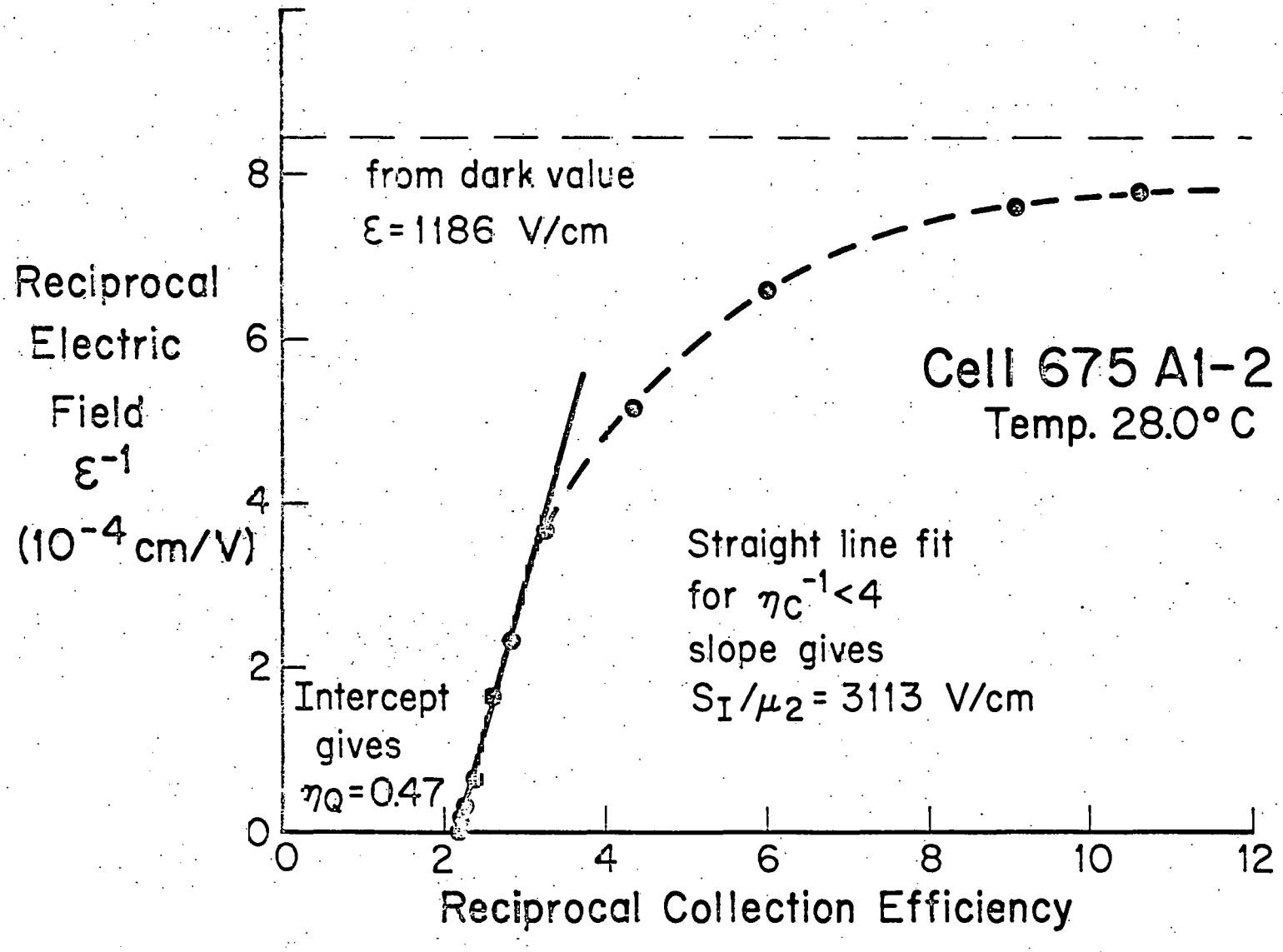

Fig. 3 Plot of reciprocal electric field versus reciprocal collection efficiency. Cell 575A1-2.

4.3.4 Phase 6 Identify Trap Levels

The use of photocapacitance to measure trap densities has continued (see Fig. 4). Preliminary measurements show that the variation of capacitance with bias voltage is complicated particularly in conjunction with the quenching experiments mentioned below. Even in the best case (AM1), $1/C^2$ vs. V does not fit a straight line except near V = 0 (typical $N_D^* = 5.2 \times 10^{16}$ cm^{-3}), see Fig. 5. Rather, the slope changes in such a way as to indicate a decrease of N_D^* farther from the junction.

In the dark, C is almost constant with V, while under some quasi monchromatic excitation, the expected decrease of C under reverse bias is actually reversed in some ranges of V. These effects will have to be interpreted in terms of: a) photogenerated carriers from the Cu_2S reaching the depletion region, b) uncovering of trap levels and interface states by the Fermi level and/or c) transitions involving trap levels.

Connected problems include the instability of conductance as the bias is varied, and the consideration of alternate (more difficult) methods of calculating C taking into account finite R_s.

After looking at transients in capacitance produced by chopping white light, it was found that better results, containing greater potential information can be obtained by quenching with long-wavelength excitation. Two-beam methods produce even better results, where the sample is excited continuously with blue light, while a second beam in the red and IR region is chopped. High-intensity bulbs followed by color-glass filters give better results than use of a grating monochromator.

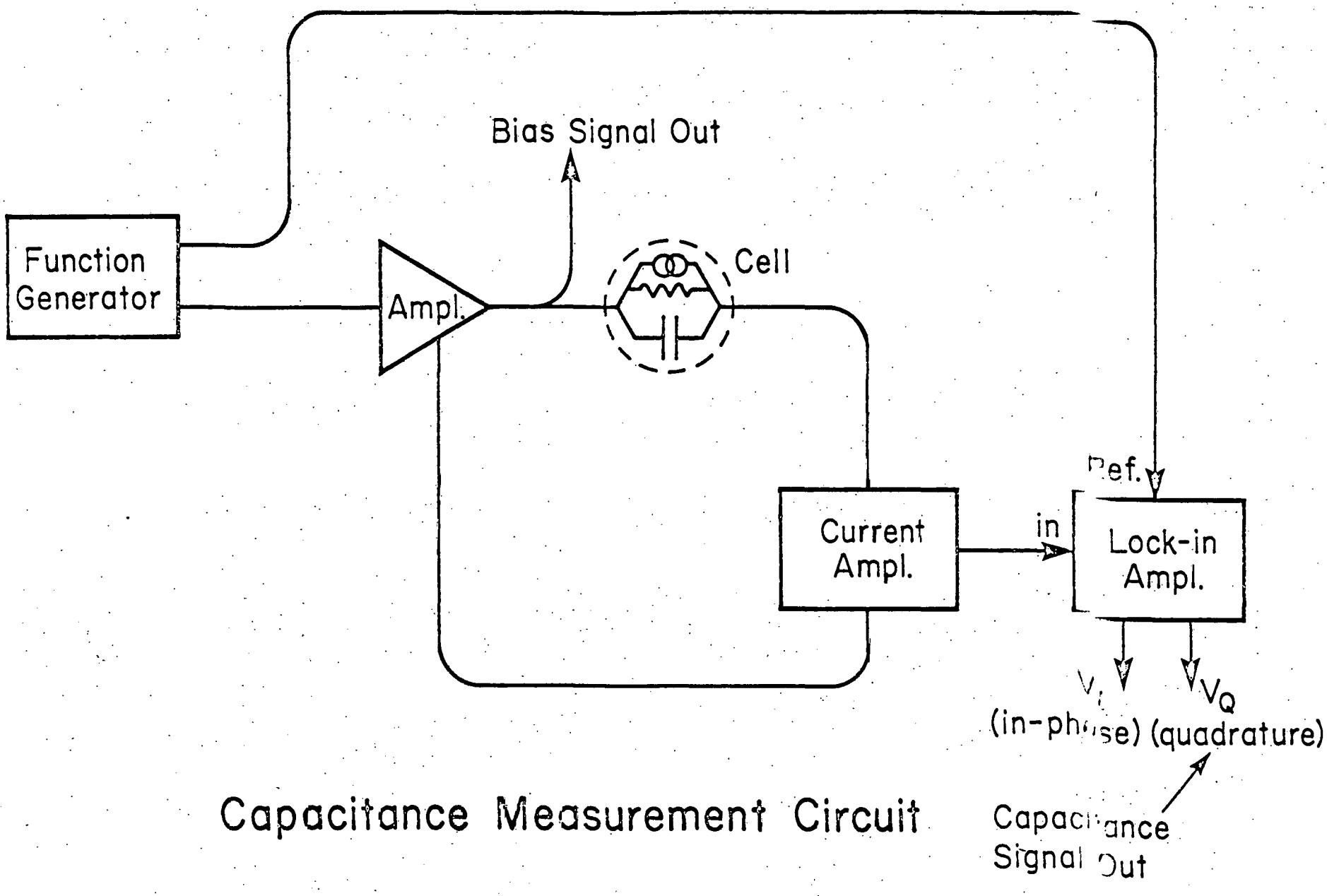

Capacitance Measurement Circuit

Fig. 4 Block diagram of capacitance measurement circuit.

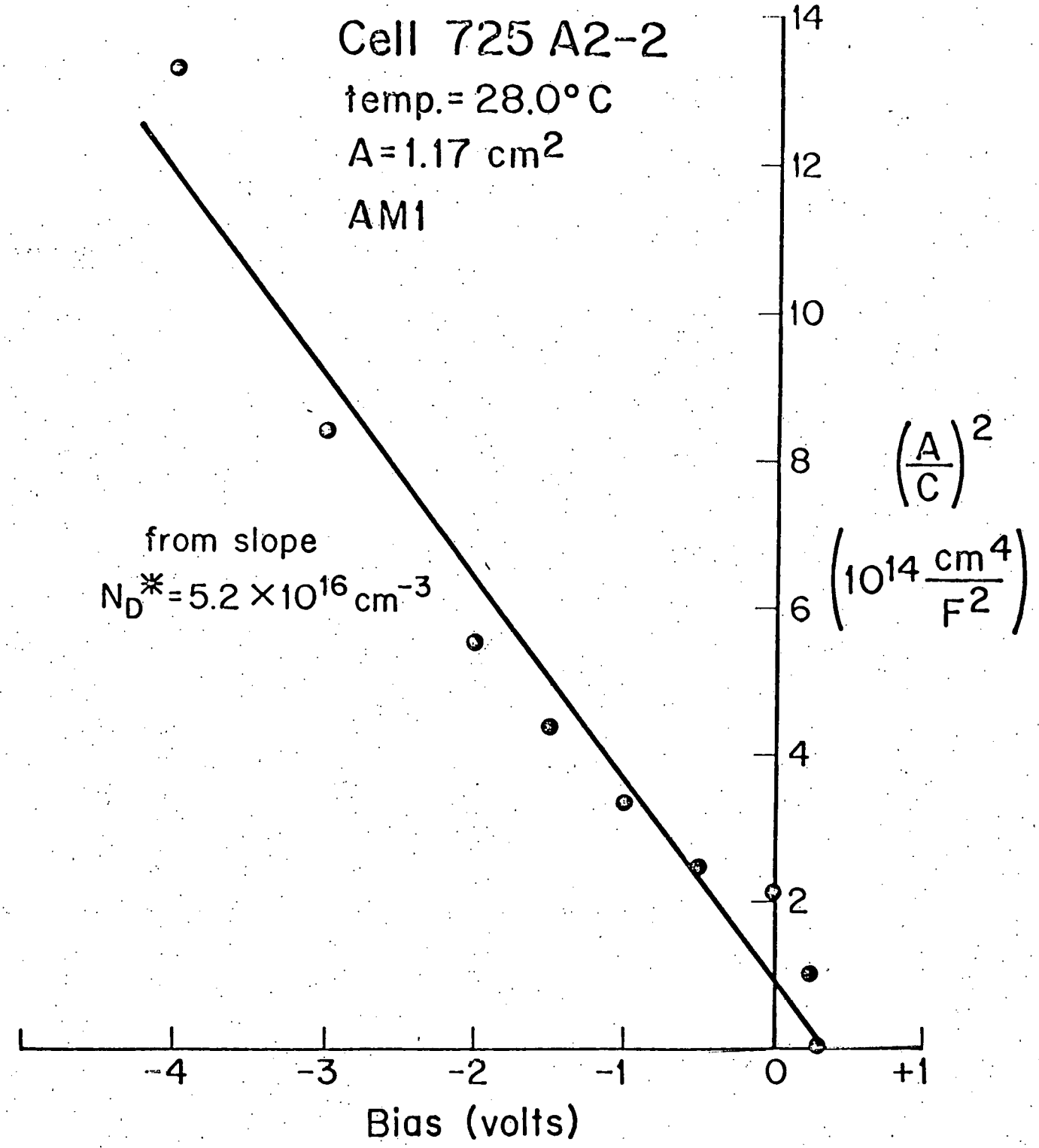

Fig. 5 Plot of $1/C^2$ versus bias voltage.

With sufficiently intense red beam, quenching can be 80% or higher. Low temperature improves quenching, but will require a controlled atmosphere. The results must be interpreted in terms of loading and unloading traps. In order to investigate the dynamics of the states, measurements have been started on the effect of varying beam intensity and on transient response. Usable traces of V_Q and V_I have been made on a chart recorder, and it has been found that the transients depart from simple exponentials even more than previously reported. A start has been made on computer analysis of these transients.

Extension of the temperature range to liquid nitrogen is planned.

4.3.5 Phase 7 Theoretical Modeling

a) In the theoretical modeling aspect of Task 3 a complete derivation of the dependence of the current voltage relation upon the value of N_A in Cu_2S and N_D in CdS was carried out. Experimental studies to verify some of the predictions were performed on special cells with very thick Cu_2S (0.85 μm) produced by the solid state reaction. Much of this work was reported in the 1979 Photovoltaic Energy Conference in Berlin. A copy of this paper is attached in Appendix C.

b) Studies of the decay of V_{oc} in (CdZn)S/Cu_2S cells coupled with the material studies that reveal deep spikes of Cu_2S forming into the (CdZn)S layer suggests the following model for the V_{oc} decay.

Under illumination, the space charge region near the junction shrinks due to the trapping of holes at copper acceptor center. This shrinking of the space charge region width would generally allow some tunneling through the junction if it proceeds far enough. Experimentally tunneling effects which

are attributed to this cause are seen under illumination with strong blue light, in which case V_{oc} drops. In strong infrared light, the space charge region does not shrink as much, and V_{oc} is observed to be larger than with either blue or white light.

For the deep fingers the amount of blue light reaching that depth is very slight. Therefore the shrinkage in the space charge region width and the higher field will not take place at these deeper fingers for a considerable time. However, once the space charge region has decreased by virtue of the holes being trapped, the current will be considerably higher because in the geometry of a point the field is much larger and hence the tunneling would be taking place to a greater extent. The tentative model is that the time dependence is associated with the narrowing of the space charge region at points which are at different depths below the junction and hence the amount of light reaching them and the time at which the tunneling takes place will vary. The marked decrease in V_{oc} is due to the fact that once tunneling begins in these regions they carry a higher current than the planar regions of the junction, and in effect have a lower barrier height causing a lower V_{oc}.

c) The work on the two dimensional aspects of sheet resistance in solar cells can be summarized as follows:

Assumptions:

1. Resistance loss in grid line, bus bar, and CdS are negligible
2. Cu_2S is uniform
3. Junction acts as ideal diode (i.e. $J = J_o \exp(\alpha V_j)$ where: $\alpha = \frac{q}{nkT}$)

Definitions: 1. $J \equiv \frac{J}{J_L + J_0}$

2. $v \equiv \alpha V$

3. $V_{oc} \equiv \text{Ln} \frac{J_L}{J_0}$

4. $r \equiv \frac{\alpha R \quad L^2(J_L + J_0)}{8}$

R = sheet resistance of Cu_2S

L = grid spacing

5. $a = \alpha\chi$

where χ is the maximum voltage drop across the Cu_2S

Equations to be solved:

1. $a - \exp(-v_{oc} + v)[\exp(a) - 1]$

2. $\int_o^a \frac{dx}{[x - \exp(-v_{oc} + v + a)(1 - \exp - x)]^{1/2}} = 2r^{1/2}$

the above set has to be solved to eliminate a to get the current voltage characteristic (i.e. $f(j,v) = 0$).

Limits on solutions:

$$j \geq 1 - \exp(-v_{oc} + v + jr)$$

This gives an upper limit to series resistance losses of the Cu_2S.

$$j \leq 1 - \exp(-v_{oc} + v + jr/2)$$

This gives a lower limit for losses; a better approximation (but more complicated) is:

$$j^2 \geq 1 - \exp(-v_{oc} + v)[(r+1) \exp j_v - 1]/r$$

$$j \leq 1 - \exp(-v_{oc} + v)(\exp jr - 1)/jr$$

All the numerical solutions used to find the maximum power point used excessive CPU time and a new iteration scheme being programmed will take care of this.

In order to study the predictions of this model and determine by direct measurement on actual cells the value of sheet resistance, an interdigitated contact has been designed. It consists of a pair of grids with equal line spacings, offset by half that spacing, each connected to separate bus bars. Measurements of cell characteristics using each grid and both together, as well as the current voltage relation with a voltage between the bus bars allow the sheet resistance and photoconductive effects to be studied.

4.4 Task 4 Encapsulation for Improved Stability

Monitoring of the roof top cells has been maintained and a third cell was added on May 9. The latter cell #695A1.4 was encapsulated between glass and a Kovar plate using Dow Corning QL2577 potting compound.

Plots of J_{sc}, V_{oc} and Efficiency are given in Figures 6 and 7 for cell 695B1.3. A preliminary interpretation of the data is that the rapid loss of performance at about day 100 corresponds to the onset of warm humid weather. This would imply that the packaging procedure is not giving a good hermetic seal.

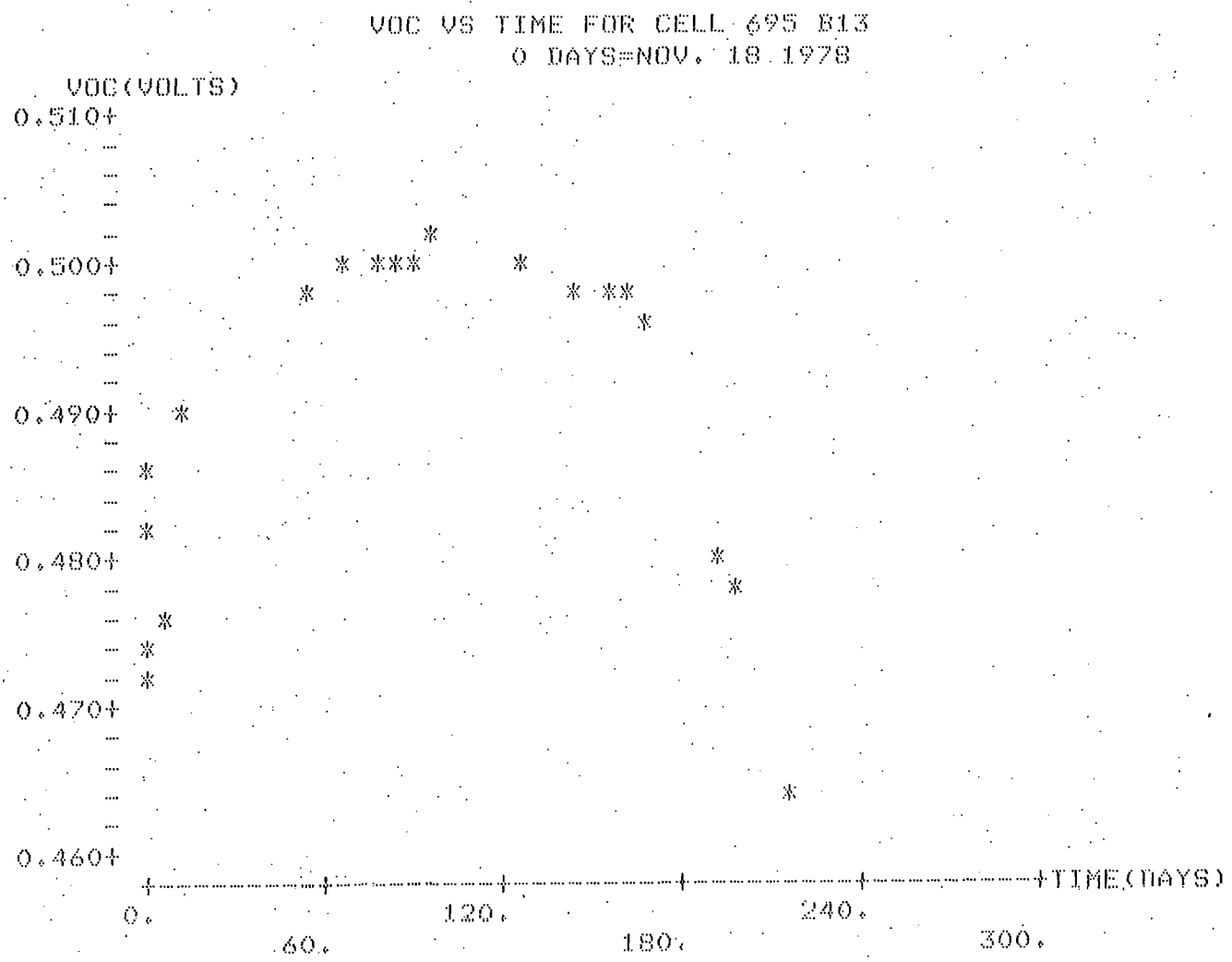

Fig. 6 Plots of open circuit voltage and short circuit current as a function of time. Cell 695.B13.

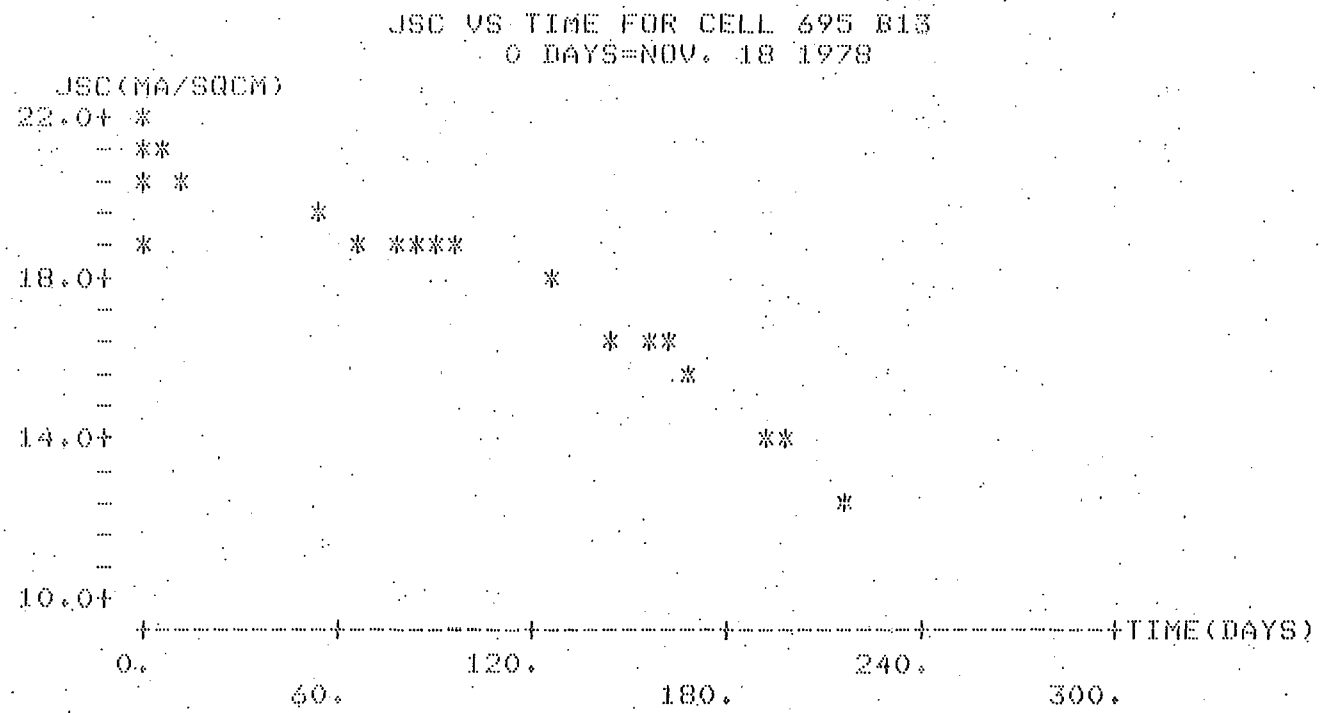
JSC VS TIME FOR CELL 695 B13
0 DAYS=NOV. 18 1978
JSC(MA/SQCM)
22.0
18.0
14.0
10.0
TIME(DAYS)
0.
60.
120.
180.
240.
300.

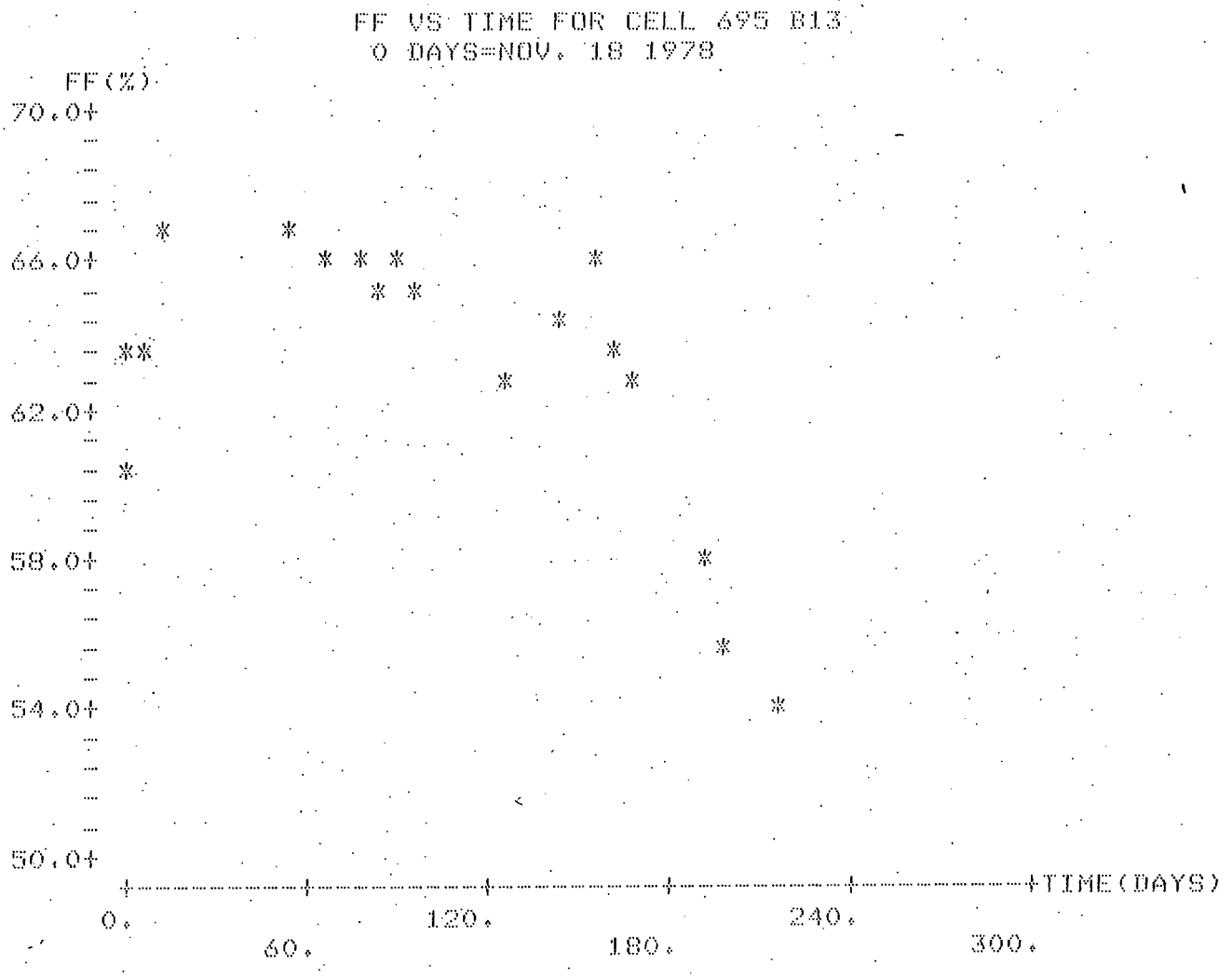

Fig. 7 Plots of fill factor and efficiency versus time. Cell 695.B13.

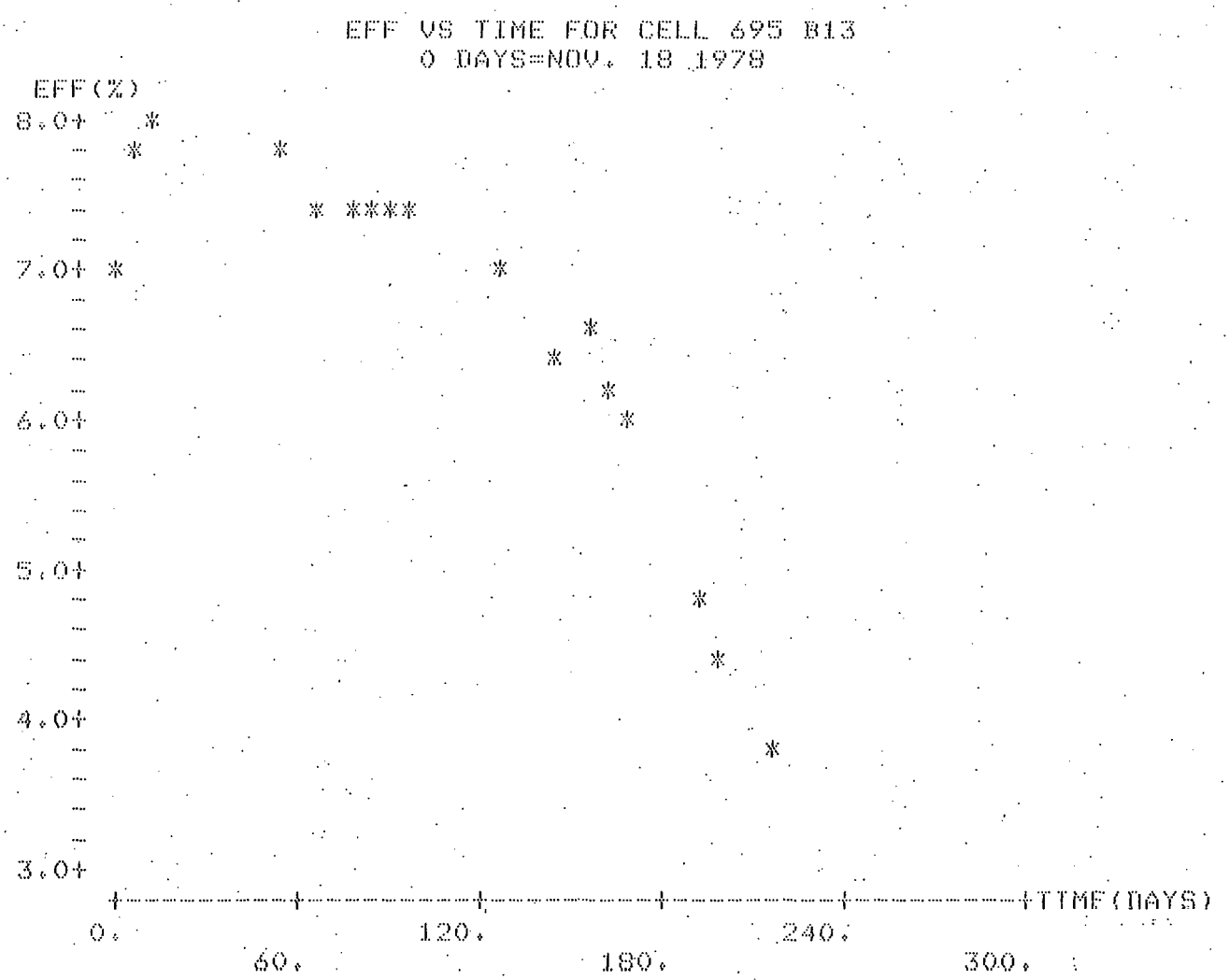
EFF VS TIME FOR CELL 695 B13
0 DAYS=NOV. 18 1978
EFF(%)
8.0
7.0
6.0
5.0
4.0
3.0
TIME(DAYS)
0.
60.
120.
180.
240.
300.

5. Future Development

In both Task 1 and Task 2 the recent results indicate that substantial improvements in efficiency should be achieved within the next quarter. A model to account for the time dependent voltage in mixed sulfide cells will be used to direct cell fabrication efforts designed to produce a junction with more stable behavior.

It is anticipated that by combining the information derived from photoluminescence and the studies of trap levels using transient capacitance, the foundation of a quantitative model of hole traps in CdS and their relation to impurities and intrinsic defects will be developed.

REFERENCES

1. T. L. Hench and R. B. Hall, Proceedings of Photovoltaic Solar Energy Conference, Berlin, 1979, p. 379 - 386.
2. A. M. Barnett, J. A. Bragagnolo, R. B. Hall, J. E. Phillips and J. D. Meakin, Proceedings 13th IEEE Photovoltaic Specialists Conference (1978), p. 419.
3. Final Report NSF/RANN/AER72 - 03478 A04 FR76, March, 1977.
4. B. Daron, A. W. Catalano and E. A. Fagen, Proceedings 13th IEEE Photovoltaic Specialist Conference (1978), p. 406
5. L. C. Burton, B. Baron, T. L. Hench and J. D. Meakin, J. Electronic Material, 7 159 (1978).
6. A. Rothwarf, Optimal Material Properties for CdS/Cu_2S Solar Cells, Proceedings of Photovoltaic Solar Energy Conference, Berlin, 1979, p. 370 - 378.

Appendix A

PHOTON LOSS ANALYSIS AND DESIGN OF THIN-FILM PLANAR JUNCTION Cu_2S/CdS DEVICES

JULIO A. BRAGAGNOLO

Institute of Energy Conversion
University of Delaware
Newark, Delaware 19711

Summary

Planar junction devices with increased open-circuit voltage and projected efficiency over 10%(1) have been obtained by solid-state reaction growth of Cu_2S on unetched CdS layers. When the morphology of the Cu_2S layer is changed, a substantial decrease in short-circuit current (J_{sc}) is observed. A quantitative photon loss analysis shows that achievable J_{sc} in present planar cells is limited by reflection and that re-emission of light after internal reflection in the cell is the primary contributor to the measured losses. Light trapping, caused by diffuse internal reflection leading to total internal reflection of outgoing photons at the outer cell boundary, reduces re-emission losses of thin-film polycrystalline CdS/Cu_2S devices to a fraction of their value for a plane-parallel multilayer device. Variations in cell morphology, leading to changes in diffuse internal reflection, can explain the observed differences in reflection losses. This analysis can be useful in developing designs and processing techniques for increased photon collection efficiency of thin-film cells.

1. INTRODUCTION

Thin-film polycrystalline cells of over 9% efficiency and AM1 short-circuit current in excess of 27 mA/cm^2 have been recently reported by the Institute of Energy Conversion of the University of Delaware (2). It has been proposed that higher open circuit voltages (V_{oc}) leading to higher conversion efficiencies could be obtained by reducing the area of the CdS/Cu_2S junction (1). This change can affect other cell characteristics, in particular its photon economy (3).

The purpose of this work is to quantify the effects of solar cell morphology on photon losses of CdS/Cu_2S devices. Total (diffuse and specular) Reflectance Spectrometry is the technique best suited for optical analysis of polycrystalline layers. Spectra for the complete cell and its constitutive layers were measured using a 4π Gier-Dunkle Integrating Sphere detector in conjunction with a Beckman DK-2A spectrophotometer and the data were used to develop a quantitative photon loss analysis.

2. DESIGN ANALYSIS OF CdS/Cu_2S CELLS

A schematic cross section of a thin-film polycrystalline CdS/Cu_2S cell is shown in figure 1. The cells are built up on a substrate of electro-formed Cu $\sim$ 30 μm thick which is plated with 0.1-0.4 μm of Zn. CdS is vapor deposited to thicknesses between 20 and 30 μm with grain sizes 1 to 5 μm. The two sides of the copper substrate have different surface morphologies resulting in significant differences in the surface area of the CdS layer and consequently, of the CdS/Cu_2S junction. Conventional textured cells are made by first etching the CdS layer, grown on the rough side of the substrate, in hydrochloric acid. The Cu_2S layer, approximately 0.1 μm thick, is formed by reaction in a cuprous ion solution. Cu_2S forms along the CdS and also penetrates down the CdS grain boundaries resulting in a much larger junction area, A_j, than the projected cell area, A_t. A smoother planar CdS/Cu_2S junction can be obtained if the Cu_2S is grown by solid-state reaction between CuCl and unetched CdS. This Cu_2S formation process eliminates grain boundary penetration. To complete the cell the top electrical contact is formed by depositing a highly transmitting (96%) Au grid onto the Cu_2S and applying an anti-reflecting (AR) coating.

In conventional, high efficiency cells the heavy texture of the Cu_2S layer results in an open-circuit voltage (V_{oc}) loss (1). This loss is given by (1) $V_{oc} = (kT/q)\ \ln\ (A_j/A_t)$, it amounts to $\sim$ 40 mV for the textured cell and is negligible for the planar junction. A summary of the open circuit voltage values achieved with CdS/Cu_2S cells having various junction

textures is given in Table I. The data shows that planar junction cells on both the rough and smooth side of the copper substrate have the capability of achieving efficiencies over 10% if the short-circuit currents, $J_{sc} \sim 26$ mA/cm^2 and fill factors ~ 0.72, typical of the textured cell can be maintained. If the only design feature that is changed is the morphology of the Cu_2S layer a substantial decrease in current is observed even though the open circuit voltage increases. To provide direction to design and technology modifications to restore the current a full quantitative analysis of the photon losses for each cell design is required.

3. PHOTON LOSS ANALYSIS

The key factor in determining J_{sc} is the photon absorption rate in the Cu_2S, in which more than 95% of the minority carriers are created. Photons can be lost to electron-hole pair creation in the Cu_2S layer by several processes. The present IEC cells have a grid designed to have values of 12.5 μm wide lines and 32 lines/cm, giving a design loss of 4%. Actual widths are generally 17-25 μm resulting in 5-8% shading losses. Photon absorption processes not resulting in electron-hole pair creation in the Cu_2S arise from Cu_2S free-carrier absorption, CdS extrinsic absorption and AR cover and substrate losses. Cu_2S free-carrier absorption has been shown to be negligible for nearly stoichiometric material (4). CdS extrinsic absorption can be neglected due to the low CdS absorption constant ~ 10 cm^{-1} for $\lambda \geq 550$ nm. Total absorptance of the AR layers used has been measured for monitor samples deposited on Corning 7059 glass slides and found not to exceed 1%. Finally, substrate absorption losses have been estimated to be $\sim 10\%$ (3). This and total reflection constitute the major photon losses in present cells.

Experimental reflectance spectra of gridded thin-film polycrystalline CdS/Cu_2S devices with various Cu_2S layer and substrate morphologies but similar Cu_2S thickness are shown in Figure 2. Thickness values refer to the "skin" of the Cu_2S layer and have been estimated from effective thicknesses measured electrochemically by cathodic stripping (5). Reflection losses decrease with increasing junction and substrate texture both before (curves 1, 2, and 3) and after (curves 4, 5, and 6) SiO_x AR coating application. The average over the solar spectrum of the reflection losses using a spectrum corresponding to AM1.5 (6) has been computed from the curves. Table II summarizes the calculated averages, together with the achieved short-circuit current J_{sc} for each cell type after SiO_x AR coating application.

To reduce the "reflection" losses from the planar cell would

appear to merely require the application of more effective anti-reflection techniques. A double layer e.g. ZnS/MgF_2 coating can be designed so as to cancel the front surface reflectance from Cu_2S at $\sim$ 500 and 750 nm. A calculation assuming a semi-infinite Cu_2S layer covered by a 0.06 μm thick ZnS layer of refractive index 2.3 and a 0.1 μm thick layer of MgF_2 of refractive index 1.39 and using literature values for the Cu_2S optical constants (8) yields curve 1 in figure 3. However, when such an AR coating is actually applied to a gridded planar junction cell (curves 2 and 3) a non-zero reflectance results which increases monotonically for $\lambda > 550$ nm. This long wave reflectance is clearly dominated by re-emitted light leaving the cell after reflection at the back contact, and not by front surface reflection.

Increasing the Cu_2S thickness is also limited as a technique to increase the photon absorption efficiency in planar junction cells. While the reflectance for $\lambda > 500$ nm is decreased by increasing the Cu_2S "skin" thickness d_1 (figure 3, curves 2,4, and 5), the condition for efficiency collection of photogenerated carriers requires that $d_1 < \frac{L_n}{2}$ where $L_n \sim 0.1$-0.3 μm is the minority carrier diffusion length in the Cu_2S (7). Cells with $d_1 \geq 0.1$ μm already show a decreasing J_{sc} presumably due to carrier losses, whereas thickness in excess of 0.15 μm are necessary to achieve losses below 10% (curve 6, figure 3). In summary, losses caused by re-emitted light after reflection at the back contact account for up to 17% of J_{sc} losses in planar junction cells and are a major obstacle to the achievement of J_{sc} comparable with that of textured junction CdS/Cu_2S cells.

The key role of the front Cu_2S surface texture in the high photon efficiency of the textured junction cell can be seen for $\lambda < 500$ nm (figure 2). There CdS absorption prevents re-emitted light from contributing and total reflectance equals that of the front cell surface which is 20% lower for the textured cell. The major part of the reflection loss however, arises from the region $\lambda > 500$ nm where for Cu_2S thicknesses ≈ 0.1 μm the contribution by re-emitted light can be substantial. As we shall see in what follows. a model of the cell as a specular, plane parallel multilayer structure yields reflectance values in total disagreement with the data for both planar and textured junction cells. The results can instead be explained by "light trapping". In this model, diffuse reflection at high angles at the Cu_2S/CdS and CdS/substrate interfaces, leads to total internal reflection of outgoing photons at the Cu_2S/Air interface. This "light trapping" decreases the re-emitted component of reflectance, enhancing absorption in the Cu_2S. The effect is minimized as either the junction or the

substrate are made more nearly planar. A quantitative analysis of reflectance which can be useful as a design tool for improved photon collection in the planar cell follows.

MODEL FOR LIGHT TRAPPING

The simplest semi-quantitative model that embodies all the features necessary to the analysis of texture effects is pictured in figure 4. In this model the Cu_2S layer (medium 1) is represented as resting on a virtual substrate (medium 2) which replaces the CdS/substrate combination of the real cell. Diffuse reflection of light will be assumed to occur at this interface with an angular distribution f (Θ), independent of the angle of incidence. The function f (Θ) reflects the morphology of both, the CdS/Cu_2S junction and the CdS/substrate interface. The Cu_2S/Air interface (01) will be assumed specular for the planar junction cell, and the calculations limited to this case. Finally, the variations in orientation and thickness of the polycrystalline layers which result in diffuse reflection will be assumed to cause incoherent addition of waves reflected from the various cell interfaces. This assumption is consistent with the absence of interference effects in reflectance. The normal incidence reflectance is then given by:

$$R = R_{01} + \frac{(1 - R_{01})\, I_1 \exp - (\alpha_1 d_1)}{1 - I_2} \qquad (1)$$

where

$$I_1 = 2\pi \int_0^{\pi/2} f(\Theta)\ [1 - R_{10}(\Theta)] \exp - \left(\frac{\alpha_1 d_1}{\cos \Theta}\right) \sin \Theta d\Theta$$

$$I_2 = 2\pi \int_0^{\pi/2} f(\Theta)\, R_{10}(\Theta) \exp - \left(\frac{2\alpha_1 d_1}{\cos \Theta}\right) \sin \Theta d\Theta$$

$$R_{01} = \frac{(1-n_1)^2}{(1+n_1)^2}$$

$$R_{10}(\Theta) = \frac{\sin^2 (\Theta - \Theta')}{\sin^2 (\Theta + \Theta')} + \frac{\tan^2 (\Theta - \Theta')}{\tan^2 (\Theta + \Theta')}$$

$$\sin \Theta' = n_1 \sin \Theta$$

and where α_1, n_1 and d_1 are the absorption constant, refractive index and thickness of the Cu_2S layer. The contribution of the Cu_2S extinction coefficient k_1 to R_{01} and $R_{10}(\Theta)$ has been neglected.

Two cases deserve attention. For a specular, plane parallel multilayer structure equation (1) becomes:

$$R = R_{01} + \frac{(1 - R_{01})^2 R_{12} \exp - (2\alpha_1 d_1)}{1 - R_{01} R_{12} \exp - (2\alpha_1 d_1)} \qquad (2)$$

where R_{12} is the normal incidence reflectance of the virtual interface. Neglecting CdS absorption and the small ($\sim$ 0.02) Cu_2S/CdS interface reflectance, R_{12} equals the reflectance of the CdS/Brass interface.† Equation (2) has been evaluated with literature values for the optical constants of Cu_2S (8) and Brass (3) for various Cu_2S thicknesses (figure 5). Calculated values of reflectance are much higher than those measured (figures 2 and 3) for either planar or textured junction cells of equivalent Cu_2S "skin" thickness. This difference can be quantitatively explained by this model of light trapping: calculating R in equation (1) using a reasonable form for $f(\theta)\alpha \cos\theta$, normalized in such a way that the total reflectance of interface (12) in the diffuse case equals its normal incidence specular value R_{12} the model yields reflectances that are drastically lower than those given by the specular approximation, but are within a few percent of the planar cell results (figure 5). This suggests that light trapping arising from substrate texture is a plausible mechanism to explain the reflectance of planar junction cells. The relative insensitivity of the computed relfectance to Cu_2S thickness, as compared to the specular case, is also in agreement with the results (figures 3 and 5). The low reflectance of the textured cell for $\lambda > 550$ nm can be qualitatively analyzed in terms of variations in $f(\theta)$ induced by CdS/Cu_2S junction texture.

CONCLUSIONS

Analysis and experiments show that cell morphology is a dominant factor in determining the optical efficiency of thin-film CdS/Cu_2S cells. The high photon efficiency of the conventional textured cell arises from both, light capture at its front surface and trapping caused by diffuse reflection at the CdS/Cu_2S and CdS/Brass interfaces. Removal of the CdS/Cu_2S junction texture, while increasing V_{oc}, introduces losses which limit the J_{sc} of planar cells to about 80% of that in textured cells.

The primary contribution to reflection losses of planar cells is re-emission of light after reflection inside the cell. A simple model for reflectance shows that light trapping limits re-emission losses of thin planar devices to a fraction of their specular value. Design and processing techniques utilizing light trapping to improve photon collection of thin-film polycrystalline CdS/Cu_2S devices are under development at IEC.

ACKNOWLEDGMENTS

Many useful discussions with A. Rothwarf and E.A. Fagen are gratefully acknowledged. J.A. Cambridge is to be thanked for assistance in

†Interdiffusion of zinc and copper produces a Brass layer during processing (3).

data taking. Special thanks are due to J.E. Phillips and J.E. Cambridge for their help with the calculations.

REFERENCES

1. A. Rothwarf and A.M. Barnett, IEEE Trans. Electron Devices, Vol. ED24, p. 381 (1977).
2. A.M. Barnett, J.A. Bragagnolo, R.B. Hall, J.E. Phillips and J.D. Meakin, Proc. 13th IEEE Photovoltaic Specialists Conference, p. 419 (1978).
3. J.A. Bragagnolo, Proc. 13th IEEE Photovoltaic Specialists Conf. p. 412 (1978).
4. B.J. Mulder, Phys. Stat. Sol. (A) 13, p. 79 (1972).
5. B. Baron, A.W. Catalano and E.A. Fagen, Proc. 13th Photovoltaic Specialists Conference, p. 406 (1978).
6. Terrestrial Photovoltaic Measurement Procedures, ERDA/NASA/1022-77/16.
7. J.J. Oakes, I.G. Greenfield & L.D. Partain, J. Appl. Phys. 48, p. 2548 (1977)
8. B.J. Mulder, Phys. Stat. Sol. (A) 18, p. 633 (1973).

Table I. Achieved V_{oc} and design analysis for CdS/Cu_2S cell.

Cell	Junction	Substrate	A_j/A_t	$V_{oc}^{\dagger}$[mV]	V_{oc}^{*}[mV]	Achievable** Efficiency[%]
690B13	Textured	Rough	10	509	513	9.6
834B14	Planar	Rough	2	545	556	10.4
686A24	Planar	Smooth	1	557	570	10.7

† Measured at maximum J_{sc}, Solar Simulator Intensity: 0.83 mW/cm^2
* Normalized to J_{sc} (AM1) = 26 mA/cm^2
** At J_{sc} (AM1) = 26 mA/cm^2, fill factor = 0.72

Table II. Average Reflectance of CdS/Cu_2S cells with SiO_x AR coating

Cell	Junction	Substrate	Reflection Loss†	J_{sc} (AM1) [mA/cm^2]
690B13	Textured	Rough	0.04 ± 0.03	24.8
686A14	Planar	Smooth	0.17 ± 0.03	20.5
462D1	Planar	Rough	0.12 ± 0.03	20.2

†After subtracting grid reflectance.

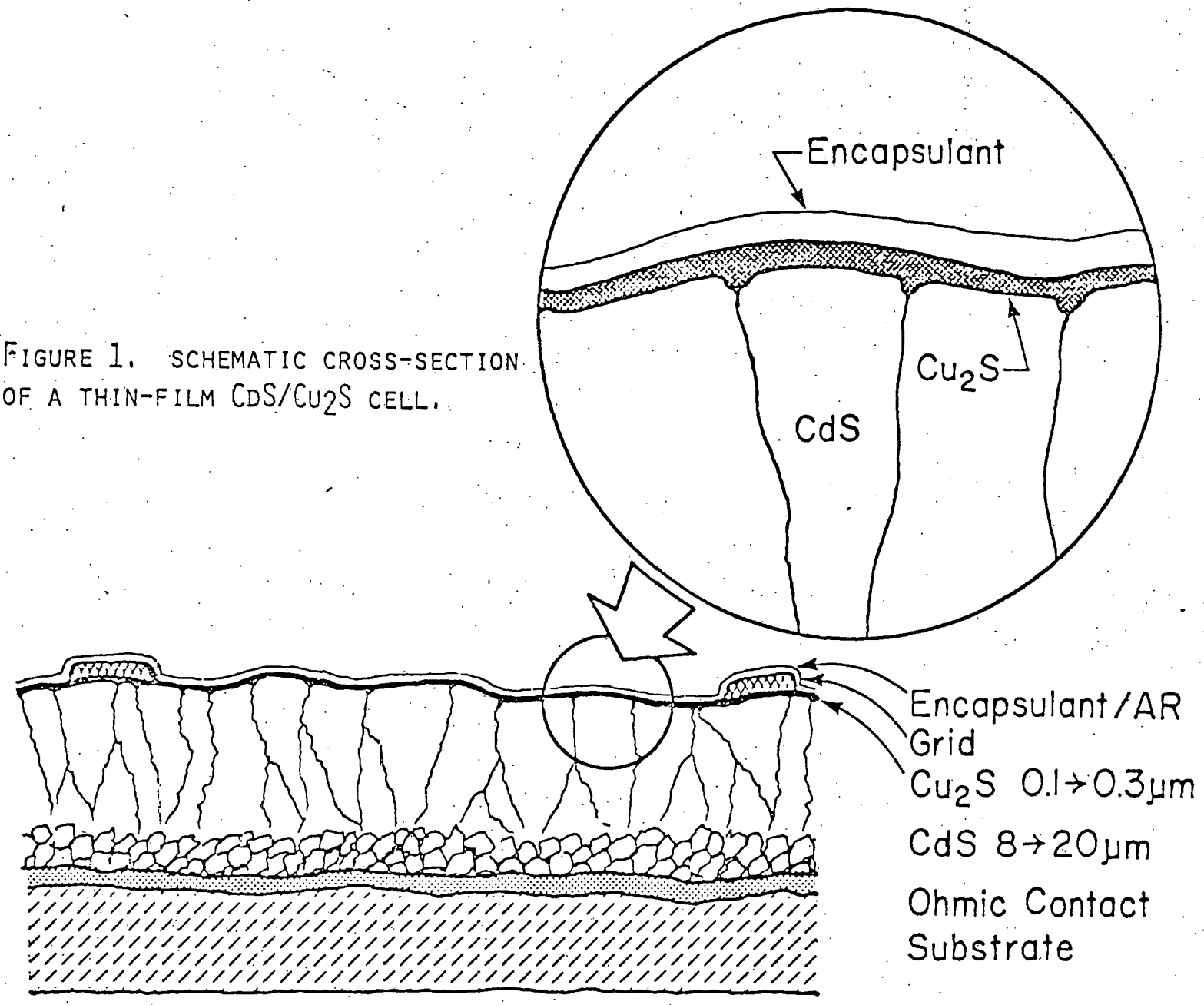

FIGURE 1. SCHEMATIC CROSS-SECTION OF A THIN-FILM CdS/Cu_2S CELL.

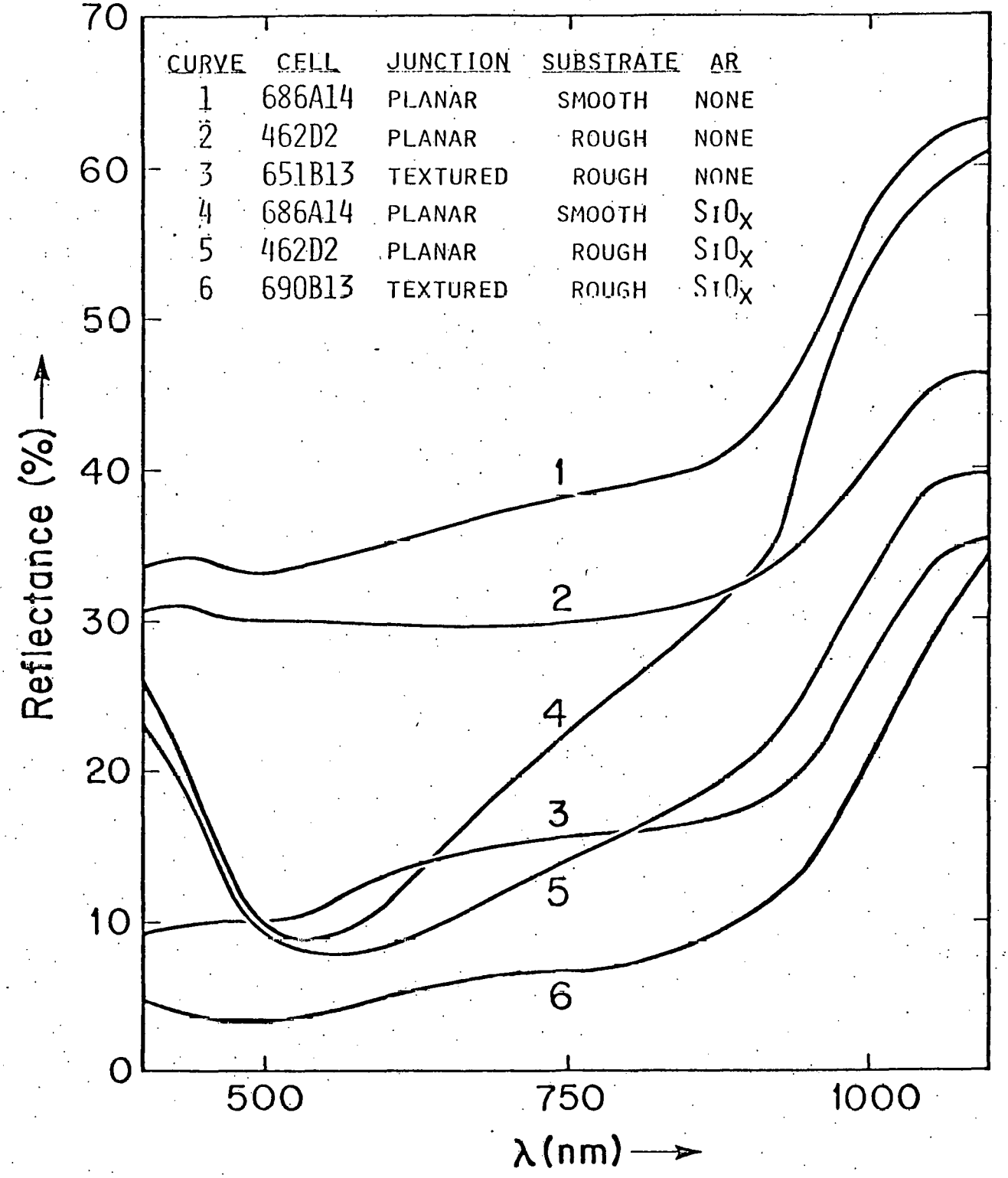

FIGURE 2. REFLECTANCE OF PLANAR AND TEXTURED CdS/Cu_2S CELLS. ESTIMATED Cu_2S "SKIN" THICKNESS ~ 0.1 μM.

FIGURE 3. REFLECTANCE OF PLANAR THIN-FILM CdS/Cu_2S CELLS.

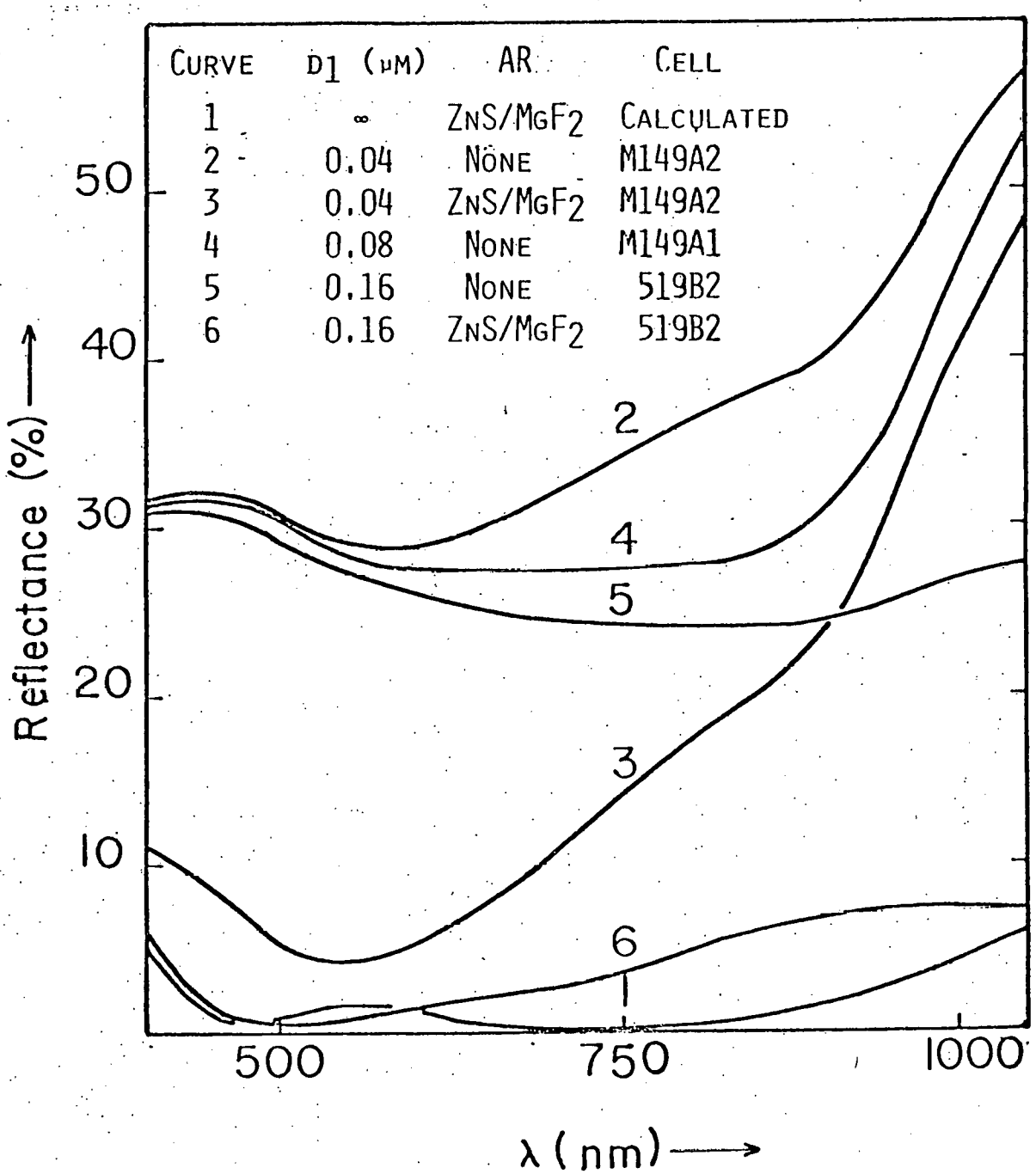

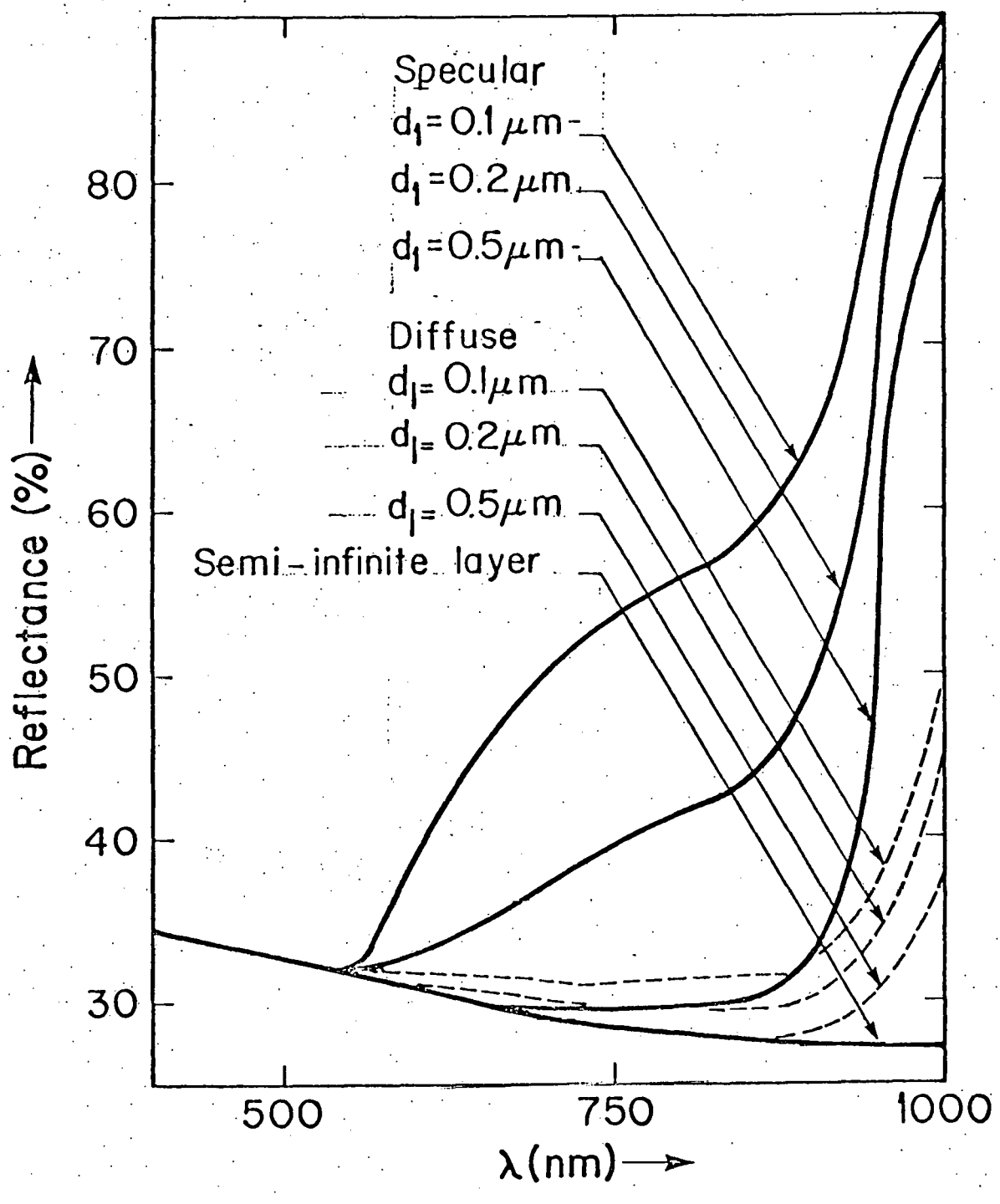

FIGURE 5. CALCULATED REFLECTANCE FOR SPECULAR AND DIFFUSE BACK REFLECTION.

Appendix B

INTERFACE RECOMBINATION AND JUNCTION FIELD STUDIES IN THE Cu_2S - CdS SOLAR CELL

LESLIE M. KILGREN

Institute of Energy Conversion
University of Delaware
Newark, DE 19711
U.S.A.

Summary

In the Cu_2S - CdS solar cell a significant part of the recombination losses are due to interface states in the junction. A technique has been developed which directly determines the voltage dependence of the interface recombination. An experiment is described which allows one to measure cell response to a modulated monochromatic source while the cell is biased with an applied voltage and illuminated by light of varying spectral content and intensity. Phase-sensitive detection is used to measure the cell response to the modulated source. It has been determined that the light-generated current is a function of the applied voltage. Also, marked differences in the fraction of current lost due to voltage-dependent junction effects have been noted for cells of differing performance characteristics. For cells of generally good performance characteristics the changes noted as a function of spectral content and intensity of the bias light are in good qualitative agreement with theoretical predictions as well as conclusions inferred from capacitance and current-voltage studies.

1. INTRODUCTION

There are many mechanisms whereby the current-collection capabilities of solar cells can be limited. Besides the design and materials-production-related losses such as grid shading, series resistance and shunt conductance, there are the more involved carrier-related phenomena of surface, bulk and interface recombination. For the case of the CdS-Cu_2S heterojunction solar cell, where the lattice mismatch is nearly 5% in two of the three dimensions, interface recombination can become the dominant mechanism controlling current flow (1). That this is the case can also be seen from barrier height measurements of these cells. Values consistently range between .85 eV and .95 eV, which are all much less than the 1.2 eV which would be required if significant numbers of carriers were passing through the junction without recombining (2). An experimental technique has been developed which separates out the voltage-dependent interface losses and quantitatively determines their significance.

2. THEORY

Following is the current-voltage relation for the CdS-Cu_2S cell:

$$J = J_0\{\exp [\frac{e}{kT}(V - JAR_S)] - 1\} - J_L$$

where J_0 is the saturation current, e is the electronic charge, k is Boltzmann's constant, T is the absolute temperature, A is the cell area, R_s is the series resistance, and J_L is the light-generated current density (3).

Varying the applied voltage across a cell will cause changes in the width of the depletion region and in the junction electric field, and hence will influence the amount of current lost due to interface recombination. The present model of cell operation states that the interface recombination depends on the field at the junction as follows:

$$J_L = J_{LO} \frac{\mu_2 F_2}{S_I + \mu_2 F_2}$$

where J_{LO} is the light-generated current density flowing into the junction from the Cu_2S, μ_2 is the electron mobility in CdS, F_2 is the electric field in the CdS at the junction, and S_I is the effective interface recombination velocity (4). The junction field itself is a function of the

illumination on the cell as well as the applied voltage across the cell. Since efficiency is related to the ratio of J_L at the maximum power point to J_L at V = 0, (5) it follows that significant progress toward the understanding of efficiency-limiting mechanisms would be realized if an experiment could be performed which would specify the voltage dependence of J_L, i.e., if an experiment could be performed which would determine the magnitude of the interface recombination current as a function of the applied voltage. In what follows we will present such an experiment.

3. EXPERIMENT

3.1 Development

Our interest is in cell behavior under normal operating conditions, but a measurement of J under AM1 bias at a given applied voltage different from zero is insufficient to determine the magnitude of J_L. If, however, with a given non-zero applied voltage across the cell we add in a small modulated signal via chopped light, then phase-sensitive-detection techniques can be used to separate out the resulting AC current j from the much larger overall DC AM1 current. We will be correct in calling this AC current j_L since only the light-generated current due to the additional chopped light will possess an AC component. Now if we have chosen this additional chopped light at a wavelength which does not affect the junction field, and we measure j_L for different applied voltages, then we have succeeded in determining $J_L(V)$, since the functional form of $J_L(V)$ will be the same as that of $j_L(V)$ for moderate light intensities. Also, if measurements of j_L in far reverse bias yield a constant, then we will be correct in calling that constant j_{LO}, and we have everything we need to determine what fraction of the light-generated current is lost due to interface recombination.

Our concern about finding a wavelength which will not cause changes in the junction field is a valid one, and the success of the above approach is dependent upon it. While actual band-to-band excitation in the CdS can occur only for wavelengths less than 515 nm and in our cells will account for less than 5% of the total collected current under AM1 bias conditions, (6) there are many states (hole traps, or deep centers) in the CdS at the junction which can be excited by a broad band of wavelengths, and which could thereby change the charge distribution within the depletion region and hence change the junction field. That there are a

significant number of these hole traps can be seen from capacitance measurements of CdS-Cu_2S cells, where the difference between light and dark capacitance can be as much as two orders of magnitude (5,7). Because of the complexity of the kinetics involved, those changes in j_L which are a result of changes in the depletion region (and hence junction field) due to excitation of these deep centers will not be in phase with the changes which result from the interface recombination losses, and we therefore have a means by which we can find the appropriate wavelength for our chopped light. All we need to do is to pick some convenient applied voltage and measure the out-of-phase component of j_L as a function of the wavelength of the chopped light. Any wavelength from the range where the out-of-phase component goes to zero will then serve our purposes. That such a wavelength range exists can be seen from data on the optical quenching of photocapacitance (2,8). Wavelengths in the 650-700 nm range suffice for our cells.

3.2 Technique

Figure I shows a schematic representation of the experimental set-up which is used. Light from a DC-powered tungsten source passes through a grating monochromater and an image of the exit slit is focused on the surface of a silvered light-chopping blade placed at 45° to the path of the incoming light beam. The transmitted beam illuminates the cell under test through an appropriate lens system. The beam reflected from the chopper is suitably monitored to give a continuous measurement of the primary beam intensity. The light-chopper control provides a reference signal for the lock-in amplifier which is used to measure the AC output of the cell. An ELH tungsten-iodide lamp driven by a stabilized DC supply provides the bias light. The cell under test is mounted on a thermoelectric temperature-controlled block with the necessary electrical connections to allow for application of a bias voltage and measurement of cell output. Output from the lock-in amplifier and the voltage-biasing power supply are fed to an x-y recorder for display.

4. RESULTS

Marked differences in the fraction of current lost due to voltage-dependent junction effects have been noted for cells of differing performance characteristics. Figure II shows J_L/J_{LO} at AM1* as a function of bias voltage for two cells of significantly different performance. A

*AM1 is set on the ELH lamp simulator using NASA standard reference cells.

table of current-voltage parameters has been included and it can be seen that while the open-circuit voltages (V_{OC}) are within 5% of each other, and the short-circuit currents (J_{sc}) are within 3%, the fill factor (FF) of cell M169B2-2 is nearly 20% less than that of cell M169B2-1. This disparity in fill factor is clearly mirrored by the J_L behavior of the two cells.

For cells of generally good performance characteristics the variation of J_L with voltage is not so pronounced under normal AM1 conditions. For these cells, however, it is possible to induce strong voltage dependence by varying the junction field via the bias light. Figure III shows J_L/J_{LO} vs. voltage for cell #810A1-4 under three different conditions of bias illumination. The top curve was taken under standard AM1, while the two bottom curves were obtained using color filters which limit the shorter wavelength portions of the spectrum.† From the included table of current-voltage parameters measured under corresponding bias light conditions we see that the J_L/J_{LO} behavior clearly mirrors the progressive loss in fill factor observed for longer wavelength illumination. This lowering of the fill factor, along with corresponding changes in photocapacitance, has been reported previously (5). Even more pronounced dependence of J_L on voltage may be observed if we reduce the junction field by lowering the intensity of the bias light. Figure IV shows corresponding data for 0.1 AM1 illumination, while Figure V shows the results for 0.01 AM1. It should be noted that as we proceed to lower and lower light intensities the difference between the two filtered measurements decreases. More specifically, adding back in some of the removed shorter wavelengths now has less of an ability to enhance J_L. This follows from the fact that the bluer light, which is better able to affect the CdS at the junction and hence modify the depletion region and the field, now has less of an effect as far as increasing J_L, since the junction field is significantly lower at the outset due to the decreased bias intensity.

5. CONCLUSIONS

Our results clearly indicate that J_L is a function of applied voltage. They are in good qualitative agreement not only with theoretical predictions of the effect of the junction field on interface recombination, but with conclusions inferred from other analysis techniques, such as current-voltage and capacitance studies. It is apparent that the present

† Corning sharp cut orange filter C.S.3-68 (507 nm $<\lambda<$ 574 nm) and sharp cut red filter C.S.2-73 (558 nm $<\lambda<$ 618 nm).

technique provides a powerful means of monitoring junction-related changes in cell response corresponding to variations in cell production parameters. We feel that further studies are extremely important in that they will aid in refinement of present theory and thereby provide insight into critical efficiency-limiting loss mechanisms. It must be stressed that previously all information about junction-related effects had to be extracted from current-voltage studies and capacitance measurements, and hence that the present work is a large step forward in that it allows for the first time direct determination of J_L as a function of applied voltage. One must also stress the broad applicability of the technique, as it can easily be applied to the study of any current-collecting photovoltaic device.

ACKNOWLEDGEMENT

James E. Phillips of the Institute of Energy Conversion is most gratefully acknowledged for his continuing contribution to this work.

REFERENCES

(1) A. Milnes and D. Feucht, "Heterojunctions and Metal-Semiconductor Junctions," Academic Press (1972).

(2) J. Lindmayer and A. Revesz, Solid State Electronics 14, 647 (1971); also, A. Potter, Jr. and R. Schalla, 6th Photovoltaic Specialists Conference, IEEE, p. 24 (1967).

(3) A. Rothwarf, Proceedings of First International Worshop on Cadmium Sulfide Solar Cells and Other Abrupt Heterojunctions, Newark, Delaware, pp. 9-50 (1975).

(4) A. Rothwarf, 13th Photovoltaic Specialists Conference, IEEE, p. 1312 (1978).

(5) A. Rothwarf, J. Phillips and N.C. Wyeth, 13th Photovoltaic Specialists Conference, IEEE, p. 399 (1978).

(6) A. Rothwarf and A.M. Barnett, IEEE Transactions on Electron Devices, ED-24, 381 (1977).

(7) H. Brandhorst, Jr., 7th Photovoltaics Specialists Conference, IEEE, p. 33 (1968).

(8) P. Lindquist and R. Bube, Journal of Applied Physics, 43, 2839 (1972).

FIGURE CAPTIONS

Figure 1. Experimental Equipment.

Figure 2. Light generated current as a function of the applied voltage for cells #M169B2-1 and #M169B2-2 at AM1 intensity.

Figure 3. Light generated current as a function of the applied voltage for cell #810A1-4 at three different bias illuminations of AM1 equivalent intensity.

Figure 4. Light generated current as a function of the applied voltage for cell #810A1-4 at three different bias illuminations of 0.1 AM1 equivalent intensity.

Figure 5. Light generated current as a function of the applied voltage for cell #810A1-4 at three different bias illuminations of 0.01 AM1 equivalent intensity.

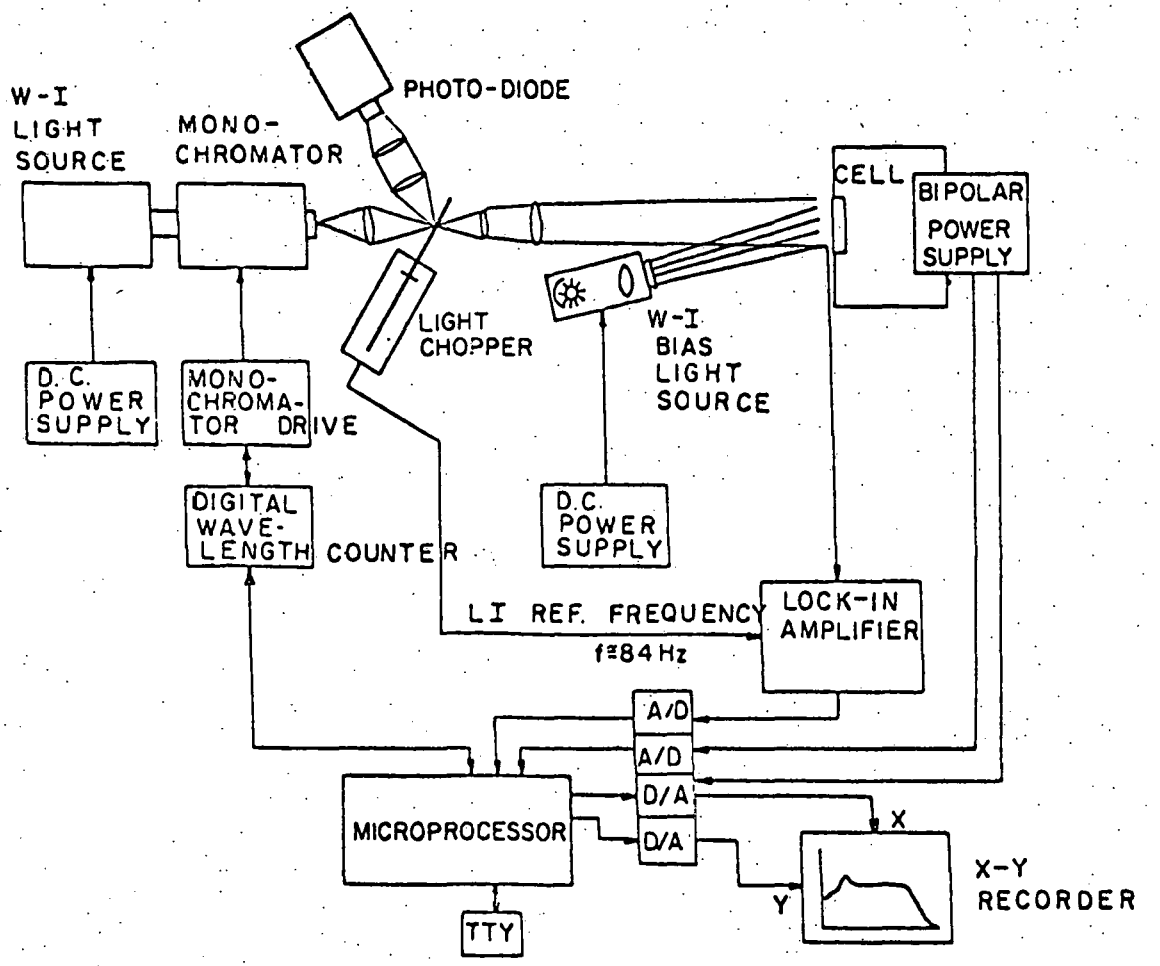
W-I
LIGHT
SOURCE
MONO-
CHROMATOR
PHOTO-DIODE
CELL
BIPOLAR
POWER
SUPPLY
LIGHT
CHOPPER
W-I
BIAS
LIGHT
SOURCE
D.C.
POWER
SUPPLY
MONO-
CHROMA-
TOR DRIVE
DIGITAL
WAVE-
LENGTH
COUNTER
D.C.
POWER
SUPPLY
LI REF. FREQUENCY
f=84 Hz
LOCK-IN
AMPLIFIER
A/D
A/D
D/A
D/A
MICROPROCESSOR
X
Y
X-Y
RECORDER
TTY

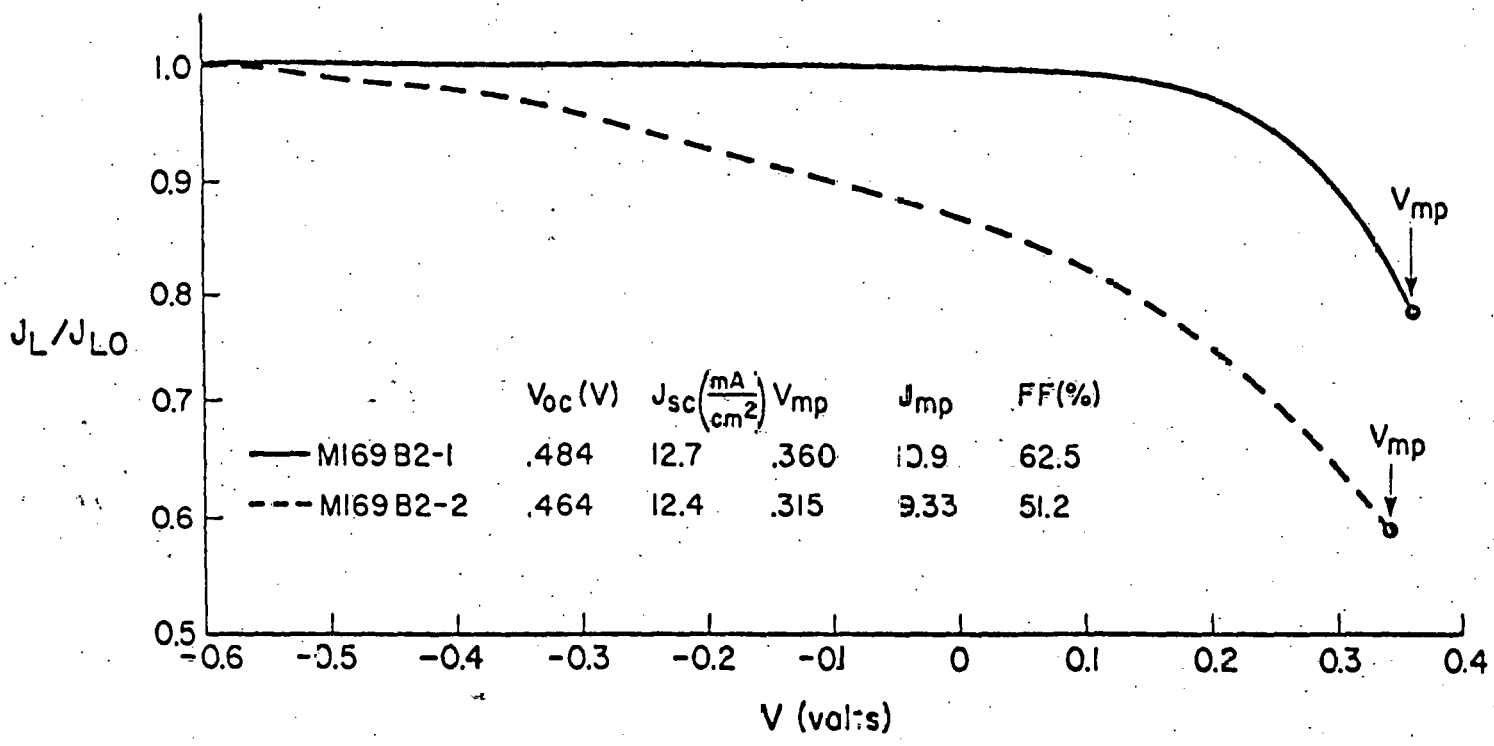
1.0
0.9
0.8
0.7
0.6
0.5
J_L/J_{LO}
V_{mp}
V_{mp}
V_{oc} (V) $J_{sc}\left(\frac{mA}{cm^2}\right)$ V_{mp} J_{mp} FF(%)
M169 B2-1 .484 12.7 .360 10.9 62.5
M169 B2-2 .464 12.4 .315 9.33 51.2
-0.6 -0.5 -0.4 -0.3 -0.2 -0.1 0 0.1 0.2 0.3 0.4
V (volts)

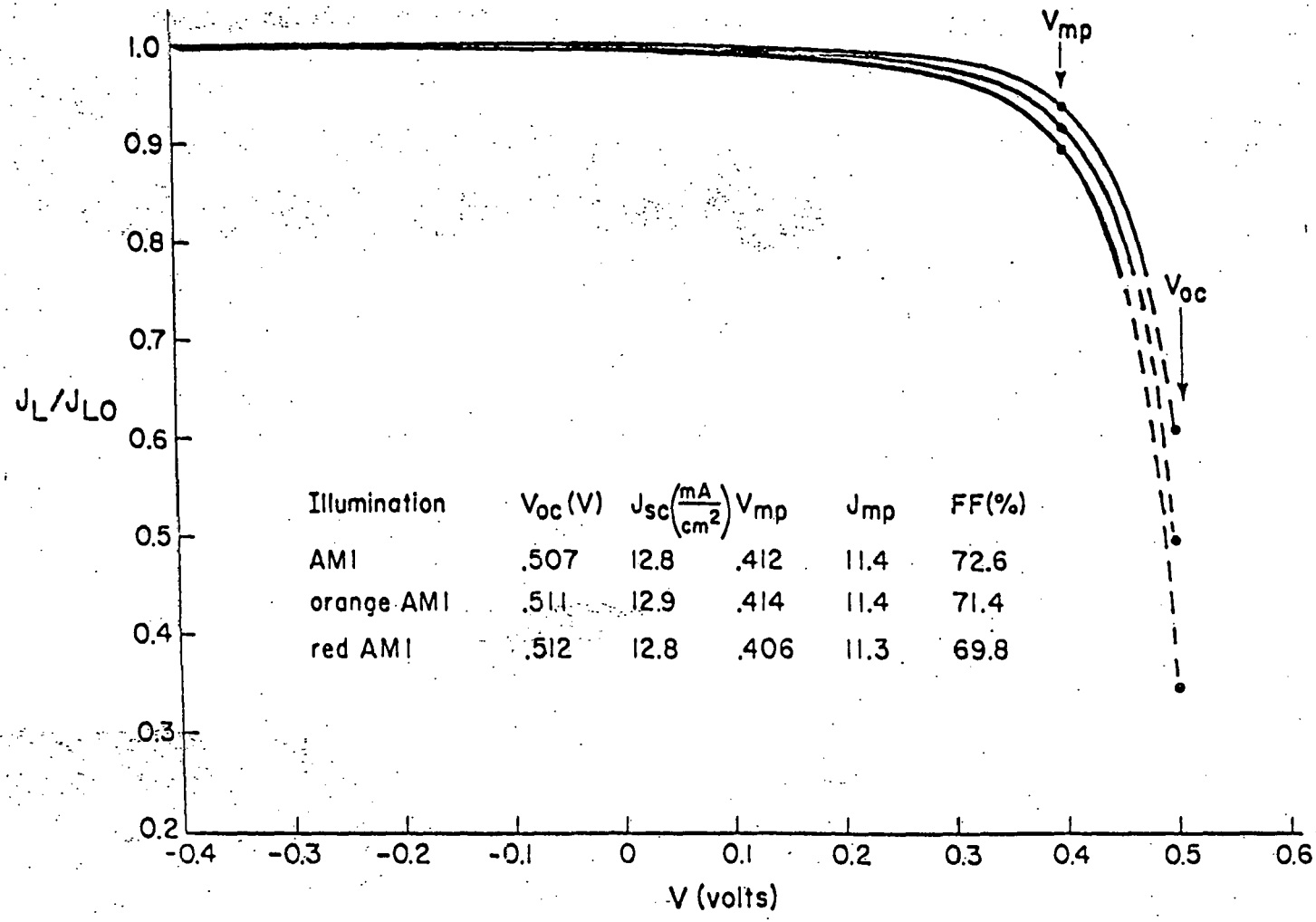

Illumination	V_{oc} (V)	$J_{sc}\left(\frac{mA}{cm^2}\right)$	V_{mp}	J_{mp}	FF(%)
AM1	.507	12.8	.412	11.4	72.6
orange AM1	.511	12.9	.414	11.4	71.4
red AM1	.512	12.8	.406	11.3	69.8

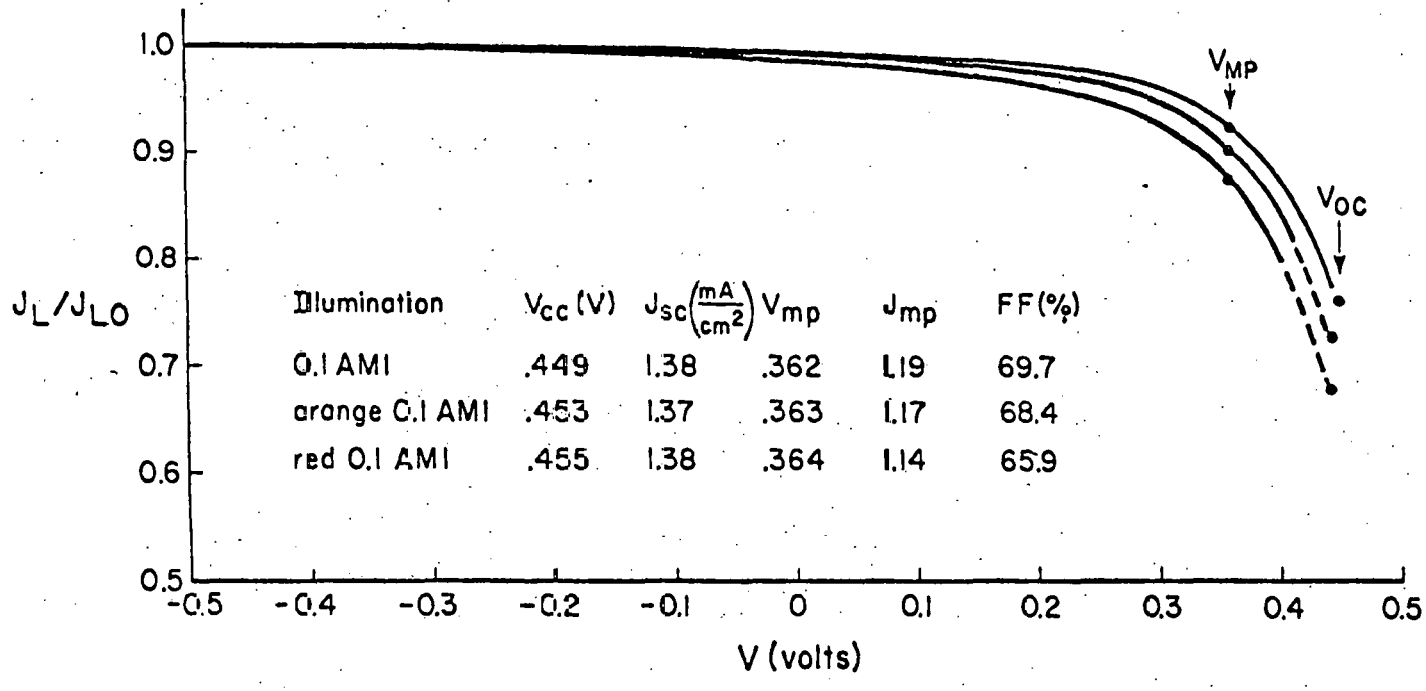

Illumination	V_{cc} (V)	$J_{sc}\left(\frac{mA}{cm^2}\right)$	V_{mp}	J_{mp}	FF(%)
0.1 AMI	.449	1.38	.362	1.19	69.7
orange 0.1 AMI	.453	1.37	.363	1.17	68.4
red 0.1 AMI	.455	1.38	.364	1.14	65.9

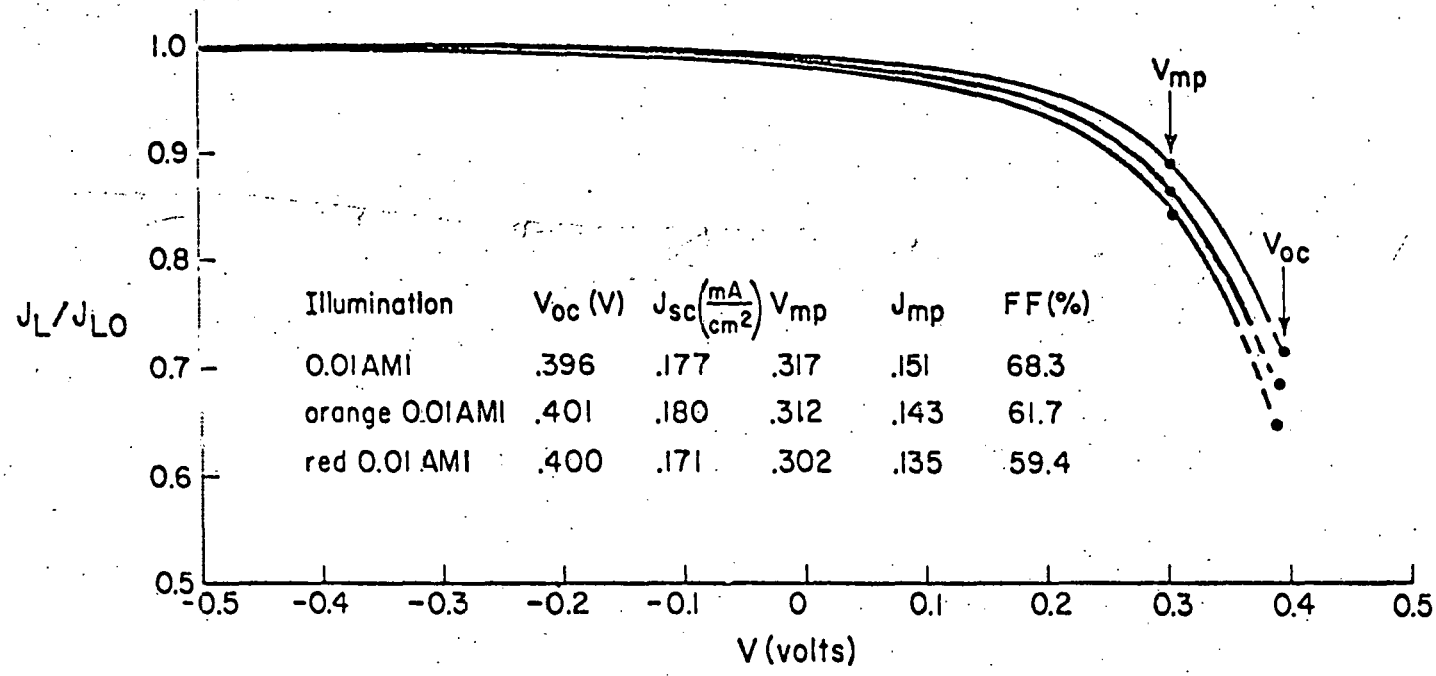

Illumination	V_{oc} (V)	$J_{sc}\left(\frac{mA}{cm^2}\right)$	V_{mp}	J_{mp}	FF (%)
0.01 AMI	.396	.177	.317	.151	68.3
orange 0.01 AMI	.401	.180	.312	.143	61.7
red 0.01 AMI	.400	.171	.302	.135	59.4

Appendix C

OPTIMAL MATERIAL PROPERTIES FOR CdS/Cu_2S SOLAR CELLS*

ALLEN ROTHWARF

Institute of Energy Conversion
University of Delaware
Newark, DE 19711 USA

1. Summary

The CdS/Cu_2S solar cell has been studied for a number of years(1). The properties reported for these cells have shown wide variations in efficiency as well as in phenomena exhibitted by the cells. The material properties of cadmium sulfide and copper sulfide have also displayed a wide variety, with significant changes in properties occuring with heat treatment of the materials.

A heterojunction model proposed previously (2) accounts for many of the properties of the cell, and has been used to guide modifications of cell production and design to achieve improved efficiency (3,4). Here we present a review of the model with emphasis on the role of the material properties of the Cu_2S and CdS layers, and experimental confirmation of predicted effects. The combined experimental and theoretical results indicate that the donor density N_D in CdS and the acceptor density N_A in Cu_2S are the crucial material properties. Optimal operation of the cell requires $N_D \simeq 10^{16} - 10^{17}/cm^3$ and $N_A \simeq 100\ N_D$.

*This work was supported in part by the Department of Energy under contract EG 77 C 03-1576.

2. THE HETEROJUNCTION MODEL AND MATERIAL PROPERTIES

The equation derived to describe the current voltage relationship of the CdS/Cu_2S solar cell is (2,3)

$$I = qA_j N_{c2} S_I \exp(-\phi/kT) \{\exp[q(V-IR_s)/AkT]-1\} - A_\perp j_{LO} \frac{\mu_2 F_2}{S_I+\mu_2 F_2} \quad (1)$$

where q is the electronic charge, and N_{c2} the effective density of states at the band edge of the CdS ($2\times10^{18}cm^{-3}$). It is based upon the band model for the cell under illumination illustrated in Fig. 1.

The parameters which are involved and the relation to material properties are as follows:

1. S_I, the interface recombination velocity is related to the misfit dislocation density at the interface between the Cu_2S and CdS due to the lattice mismatch Δa across the junction. S_I is given by the relation $S_I = V_{th}\sigma N_I^*$ where $N_I^* = 2\,\Delta a/a^3$ is the effective density of interface states and σ the capture cross section of the interface states. The expected range of S_I is 10^5-5×10^6 cm/sec.

2. $A_j/A_\perp$ is the ratio of the junction area to the planar area of the cell; and depends on the grain size in the CdS and the method of preparation of the Cu_2S: $A_j/A_\perp$ ranges from 1 to greater than 10, and reduces the open circuit voltage by an amount(5) $\Delta V_{OC} = (AkT/q) \ln A_j/A_\perp$. Two effects influence the junction area. One arises from intentional texturing of the surface with $A_j/A_\perp \sim 2.5$; the other from the formation of Cu_2S down grain boundaries, cracks, or other defects in the CdS layer. By use of CdS grown on a smooth substrate and forming the Cu_2S by a solid state reaction (CuCl on CdS), on the untextured surface $A_j/A_\perp$ is near unity and the measured V_{OC} is increased by 0.06 V. The planar structure is more highly reflecting from the front surface (6) and does not trap light effectively(7).

3. ϕ is the activation energy or barrier height to electron flow between the CdS and Cu_2S sides of the junction. It depends on the bandgap of the copper sulfide, the difference in the electron affinity between the two materials, $\Delta\chi$, the position of the Fermi level in the Cu_2S and the extent of band bending in Cu_2S. The latter two parameters in turn depend upon the density of carriers in Cu_2S and the ratio of the density of carriers in CdS, N_D to the density in Cu_2S, N_A. The equations of importance are (2):

$$\phi = Eg_1 - qV_{Dp} - \delta_1 - \Delta\chi = (Eg_1 - \Delta\chi - \delta_1 + \delta_2(A-1))/A \quad (2)$$

$$\delta_1 = kT \ln \frac{N_v}{N_A}; \quad \delta_2 = kT \ln \frac{N_{c2}}{N_D}, \quad A = \frac{N_A + N_D}{N_A} \quad (3)$$

$$V_{Dp} = V_D \frac{N_D}{N_A + N_D} = V_D \frac{(A-1)}{A} \quad (4)$$

$$V_D = Eg_1 - \Delta\chi - \delta_1 - \delta_2 \quad (5)$$

$$qV_{oc} = A\,(\phi + kT\,\ln A_{\perp} j_L/q\,N_{c2}S_I A_j) \quad (6)$$

The maximum value for ϕ for non-degenerate Cu_2S is ~1 eV when V_{DP} and δ_1 are zero, and as low as 0.5 eV depending upon the values of N_A in Cu_2S and N_D in CdS. For degenerate Cu_2S ($p \gtrsim 10^{19}/cm^3$), δ_1 will be negative and ϕ can exceed $Eg_1 - \Delta\chi$. The upper values of $\phi \simeq 1$ eV, reported on cells, may include a small contribution from negative δ_1 values.

4. A - The diode ideality factor depends directly upon the ratio of the carrier concentration in the Cu_2S and the CdS, or assuming the acceptors and donors to be fully ionized N_D/N_A. The expression for A is given in eq (3) for $N_A \geq N_D$. Hence A ranges between 1 and 2.

5. R_S is the series resistance to the extent that a series resistance written in the form given in Eq. (1) is representative of the effects of resistivity in the various layers. An adequate expression for R_S is(8) $R_S A_{\perp} = \rho_1 s^2/12 d_1$, with ρ_1 the resistivity of the Cu_2S layer, d_1 its thickness and s the spacing between parallel grid line. The values of ρ_1/d_1 the sheet resistance in good cells are $3 - 10 \times 10^3$ ohms per square. The sheet resistance depends very strongly upon the formation of a thin copper oxide layer on the surface of the Cu_2S(9). Since the oxide thickness seems to be self limiting the magnitude of ρ_1 is determined by the thickness of the underlying Cu_2S layer. The grid spacing (4) that gives optimal shading and fill factor goes as $(\rho_1/d_1)^{-1/3}$. The property of the cell affected directly by R_S is the fill factor FF. The loss in FF associated with R_S(4) is

$$\Delta FF_{R_S} = - \frac{c}{V_{OC}}\, j_{SC} R_S A_{\perp} \quad (7)$$

where c is ~0.9. However, other terms particularly the voltage dependent part of j_L can influence FF as strongly as R_S. In Fig. 2 we have plotted the theoretical dependence of FF on N_A with $V_{OC} = 0.5$ V, $\mu_1 = 6$ cm^2/V sec and $s = 3.2 \times 10^{-2}$ cm, assuming a loss of 0.05 from the voltage dependence of j_L. Table I illustrates effects of heat treatment on the fill factor and other cell parameters.

6. J_{LO} is the light generated current density arriving at the junction. Theoretical expressions for J_{LO} in terms of the modes of operation of the cell, absorption coefficient, thickness of the layers, and diffusion length have been derived and presented elsewhere (3).

Fig. 3 shows the collection efficiency, η_{coll}, and j_{L0} is the integral of η_{coll} over the appropriate wavelength range, allowing for reflection and grid absorption losses at the front surface. Experimentally, reducing heat treatments in H_2-Ar or CO increases the short circuit current, while heating in air or allowing the cell to remain unprotected in air decreases the short circuit current. The changes are reversible (see Table I). The sheet resistance of the Cu_2S is also modified. The strong dependence of both j_{SC} and the sheet resistance on stoichiometry is well documented (10) and may result from modifications in the absorption coefficient, (11) the lifetime, or the electron mobility (12). Diffusion length values are on the order of 0.3 μm (13,14) with one report of 2.7 μm (15). Comparison of experimental and calculated spectral response curves indicate that our cells have $L \leq 0.3$ μm (5).

7. μ_2 is the electron mobility in the CdS layer near the interface. It can depend upon impurity levels in the CdS, dislocation densities, grain size, stacking faults, etc. μ_2 is expected to range from the 300 cm^2/V sec seen in single crystal material down to as low as 20 cm^2/V reported in polycrystalline material (16). The true mobility in polycrystalline films is obscured by difficulties in interpreting Hall measurements and because the resistivity may vary through the thickness of the layer.

8. F_2, the junction field is given by $F_2 = (2_q V_D N_D^*/\varepsilon\varepsilon_o A)^{\frac{1}{2}}$, with N_D^* the effective donor density in CdS (4,17). The ionization state of the deep levels in CdS as determined by the light reaching them controls N_D^*, and hence F_2. In Fig. 4 current-voltage curves under various spectral illuminations are illustrated and Table II lists the corresponding photocapacitance and F_2 values. Both the capacitance and collection efficiency have been shown to be dependent (17) upon the intensity and spectral content of the light reaching the CdS layer. Photocapacitance and collection efficiency experiments (17) have established the accuracy of the F_2 term in Eq. (1). The results yield typical S_I values of 3×10^5 cm/sec, assuming $\mu_2 = 100$ cm^2/V sec.

3. INTERRELATIONSHIPS OF CELL AND MATERIALS PROPERTIES

In this section the detailed relations between the cell parameters j_{SC}, V_{OC} and FF and the material properties of Cu_2S and CdS are treated.

A. Short circuit current - J_{SC} is the last term in Eq. (1), thus we can write an expression for the expected short circuit current as a function

of both N_D and N_A, and in Fig. 5 we have illustrated a plot of j_{SC} versus N_D assuming j_{LO} = 20 mA/cm^2 for $N_A = 10^{19}$/cm^3 and j_{LO} = 15 mA/cm^2 for $N_A = 2 \times 10^{19}$/cm^3, based on Table I.

B. Open-circuit voltage. V_{OC} is given by Eq. (6). Fig. 6 indicates the dependence of V_{OC} on both N_A and N_D. The bars are the best values of V_{OC} taken from the literature (18), with the corresponding donor density deduced from the resistivity reported (μ_2 = 100 cm^2/V sec assumed). Values for recent IEC cells are indicated by ■.

In Fig. 7 we show the current-voltage relationship for a cell made with very thick Cu_2S, 0.85 μm as compared to 0.1-0.3 μm used in ordinary cells. While the thick layer cell is clearly not of interest for high efficiency its properties allow us to test key features of the model. The thick layer minimizes the effect of the thin natural oxide layer which is built up on the cell when it is exposed to air. Consequently the copper sulfide has high stoichiometry and the open circuit voltage of the cell (curve 1) is extremely low. The air and H_2-Ar heat treatments modify N_A through the Cu_2O surface layer; changing V_{OC} in accord with Eq (6). Similar curves were reported by TeVelde (19).

When cell 748A1-2 had an AM1, V_{OC} value of 0.368 V and j_{SC} = 1.4 mA/cm^2 its I-V characteristics at various white light intensities (.1-1 AM1) were obtained. From the V_{OC} vs ln intensity plot an A-factor of 1.3 was deduced. Since ρ_2 for this cell was 1.1 ohm-cm, $N_D \sim 5.7 \times 10^{16}$/cm^3 is deduced and hence $N_A = 1.9 \times 10^{17}$/cm^3. The observed value of V_{OC} agrees quite well with the 0.39 V predicted by Eq. (6) using $S_I = 3 \times 10^5$ cm/sec and $A_j/A_\perp = 1$.

The variation in reverse bias illustrated in Fig. 7 stems from the fact that j_{LO} becomes voltage dependent due to the higher collection in the space charge region on the Cu_2S side of the junction.

C. Fill Factor. The primary dependence of the fill factor on N_A is given by Eq. (7) and Fig. 2. The fill factor also depends on N_A due to band bending in Cu_2S which tends to cause a greater current collection. FF depends upon N_D and the charged acceptor levels in CdS through the effect illustrated in Fig. 4.

4. OPTIMAL MATERIAL PROPERTIES

There are six material properties of interest. In Cu_2S in addition to N_A, μ_n which affects the diffusion length and μ_p the series resistance

are important. If μ_p were greater than the 2-10 cm^2/V sec range (12) and μ_n scaled with μ_p thicker Cu_2S could be used to obtain higher efficiency cells. In CdS, N_D, μ_2 and the deep level acceptor density N_{A2} together affect V_{OC}, j_{SC}, and FF, with $N_D \sim N_{A2}$ and $N_D^* = N_D$ assumed at AM1 intensities. In present cells the μ's are not controlled. N_D is determined by growth conditions, with N_A and N_{A2} controlled by heat treatments. The calculated and experimental results indicate that for high efficiency cells $N_D \sim 10^{16} - 10^{17}/cm^3$, ($\rho_2$ = 1-10 ohm-cm), and $N_A = 100\ N_D$, (ρ_1 = 0.1-1 ohm-cm). This corresponds to Cu_xS with x 1.9995 - 1.99995. The thickness of Cu_xS indicated (neglecting that in grain boundaries) is 0.1 μm.

That this range of properties produce high efficiency cells (20) is illustrated in Table III.

REFERENCES

1. A.G. Stanley, Applied Solid State Science 5, 251-366, Academic Press 1975. A review of work through 1973.
2. A.L. Milnes, D.L. Feucht, Heterojunctions and Metal-Semiconductor Junctions, Academic Press, NY, 1972.
3. A. Rothwarf, International Workshop on Cadmium Sulfide Solar Cells and Other Abrupt Heterojunctions, Univ. of Delaware, May 1975, NSF-RANN AER 75-15858, pp. 9-50. A. Rothwarf, L. Burton, H. Hadley, G.M. Storti, Conference Record 11th IEEE Photovoltaic Specialist Conf. Scottsdale, Arizona, May 1975, p. 476-481.
4. A. Rothwarf, A.M. Barnett, IEEE Transactions on Electron Devices ED-24, 381-387, 1977.
5. A. Rothwarf, Conference Record 12th IEEE Photovoltaic Specialists Conf. Baton Rouge, LA, Nov. 1976, 488-495. A. Rothwarf, Proceedings of International Conference on Solar Electricity, Toulouse France, 1976,p. 273-284.
6. J.A. Bragagnolo, Conference Record 13th Photovoltaic Specialists Conf. Washington, DC, June 1978, p. 412-416.
7. J.A. Bragagnolo, This conference.
8. N.C. Wyeth, Solid State Electronics 20, 629-634 (1977).
9. B. Baron, A.W. Catalano, E.A. Fagen, Conf. Record 13th IEEE Photovoltaic Specialists Conf., Washington, DC, June 1978, p. 406-410.
10. W. Palz, J. Besson, T. Nguyen Duy, J. Vedel Conference Record 9th IEEE Photovoltaic Specialist Conf. Silver Spring, Maryland, May 1972, p. 91.
11. L.C. Burton, H. Windawi, J. Appl. Phys. 47, 4621 (1976); B.J. Mulder, Phys. Status Solidi (a) 13, 79 (1972).
12. G.Z. Idrichan, G.P. Sorokin, Inorganic Materials 11, 1449 (1975). F. Gaustavino, H. Luquet, J. Bougnot, Proc. of Photovoltaic Power and its Application in Space & on Earth, International Congress, The Sun in the Service of Mankind, Paris, 1973, p. 190.
13. W.D. Gill, R.H. Bube, J. Appl. Phys. 41, 1694 (1970).
14. J.J. Oakes, J.G. Greenfield, L.D. Partain, J. Appl. Phys. 48, 2548 (1977).
15. P. Leitz, G. Marchal, W. Palz, D. Nguyen, Proceedings of International Conference on the Physics and Chemistry of Semiconductor Heterojunctions and Layer Structure, Budapest Oct. 1970, Vol. II p. 385-396.

16. L.L. Kazmerski, W.B. Berry, C.W. Allen, Conference Record 8th IEEE Photovoltaic Specialists Conference, Seattle, WA Aug. 1970, p. 9-12.
17. A. Rothwarf, J. Phillips, N. C. Wyeth, Conference Record 13th IEEE Photovoltaic Specialist Conference, Washington, DC, June 1978, p. 399-405.
18. W. Palz, G. Cohen Solal, J. Vedel, J. Fremy, D.T. Nguyen, J. Valerio, Conference Record, 7th IEEE Photovoltaic Specialist Conference, Pasadena, CA, Nov. 1968, 54-61.
19. T.S. LeVelde, Solid State Electronics 16, 1305-1314, (1973).
20. A.M. Barnett, J.A. Bragagnolo, R.B. Hall, J.E. Phillips, J.D. Meakin, Conference Record 13th Photovoltaic Specialists Conference, Washington DC, June 1978, p. 419-420.

Table I. Effects of Heat Treatment on Cell Parameters at Simulated AM1

Cell	j_{SC}(mA/cm^2)	V_{OC}	FF(%)	η(%)	d_1(μm)	ρ_1/d_1(ohm)	Heating
393C2	14.9	0.500	71.9	5.4	0.19	6 x 10^3	H_2Ar 120°C
ρ=2.3	9.3	0.471	69.2	3.0	0.19	2.4 x 10^3	Air 150°C
581A2-1	20.1	0.502	72.1	7.27	0.36		
ρ=7.8	14.8	0.498	73.8	5.42	0.36		Air 170°C
	21.4	0.491	67.1	7.06	0.36		H_2-Ar 170°C

Table III. Characteristics of High Efficiency Cells Under Collimated Sunlight Illumination

Cell	j_{SC}(mA/cm^2	V_{OC}	FF(%)	η(%)	d_1(μm)	Area (cm^2)	Intensity mW/cm^2
690B1-3 ρ=4.8	21.8	.516	71.4	9.15	0.3	0.884	87.9
695A1-4 ρ=1.8	20.8	.500	73.1	8.88	0.3	1.26	85.7

Table II. Fill Factor and Photocapacitance Changes With Spectral Content. Cell 675B1-4 ρ=8.3 ohm-cm

Illumination	FF(%)	C/A nF/cm^2	F_2 (10^4V/cm)
AM1 (ELH Lamp)	66.2	46.8	7.9
Blue λ<0.59 um	67.7	45.8	7.7
Orange λ>0.54 μm	61.2	18.7	3.2
Red λ>0.58 μm	56.9	16.0	2.7

FIGURE CAPTIONS

Fig. 1. Band diagram of the CdS/Cu_2S solar cell under illumination.
Fig. 2. The calculated fill factor of the Cu_2S solar cell as a function of carrier concentration in Cu_2S ($p = N_A$)
Fig. 3. Calculated collection efficiency $j_{SC}/q\phi$ (λ) as a function of absorption coefficient α, thickness d, diffusion length L, and surface recombination velocity S.
Fig. 4. Current voltage curves for cell 675 B1-4 indicating dependence upon spectral content of illumination (see Table II).
Fig. 5. Calculated dependence of j_{SC} on the donor density N_D in CdS, with $S_I = 10^6$ cm/sec.
Fig. 6. Calculated dependence of V_{OC} on N_A and N_D with experimental data.
Fig. 7. Current voltage curves of special CdS/Cu_2S cell illustrating pronounced effect of heat treatments on cell characteristics.

Fig 1

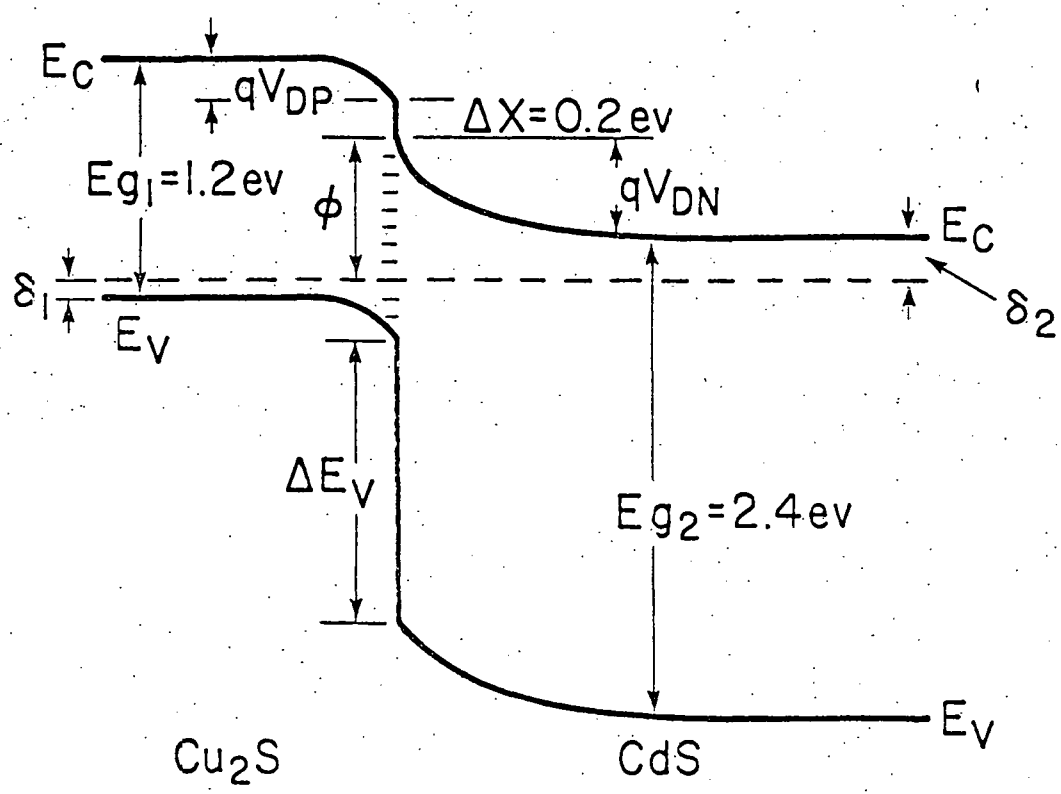
E_C
qV_{DP}
$\Delta X = 0.2$ ev
$Eg_1 = 1.2$ ev
ϕ
qV_{DN}
E_C
δ_1
δ_2
E_V
ΔE_V
$Eg_2 = 2.4$ ev
E_V
Cu_2S
CdS

Fig 2

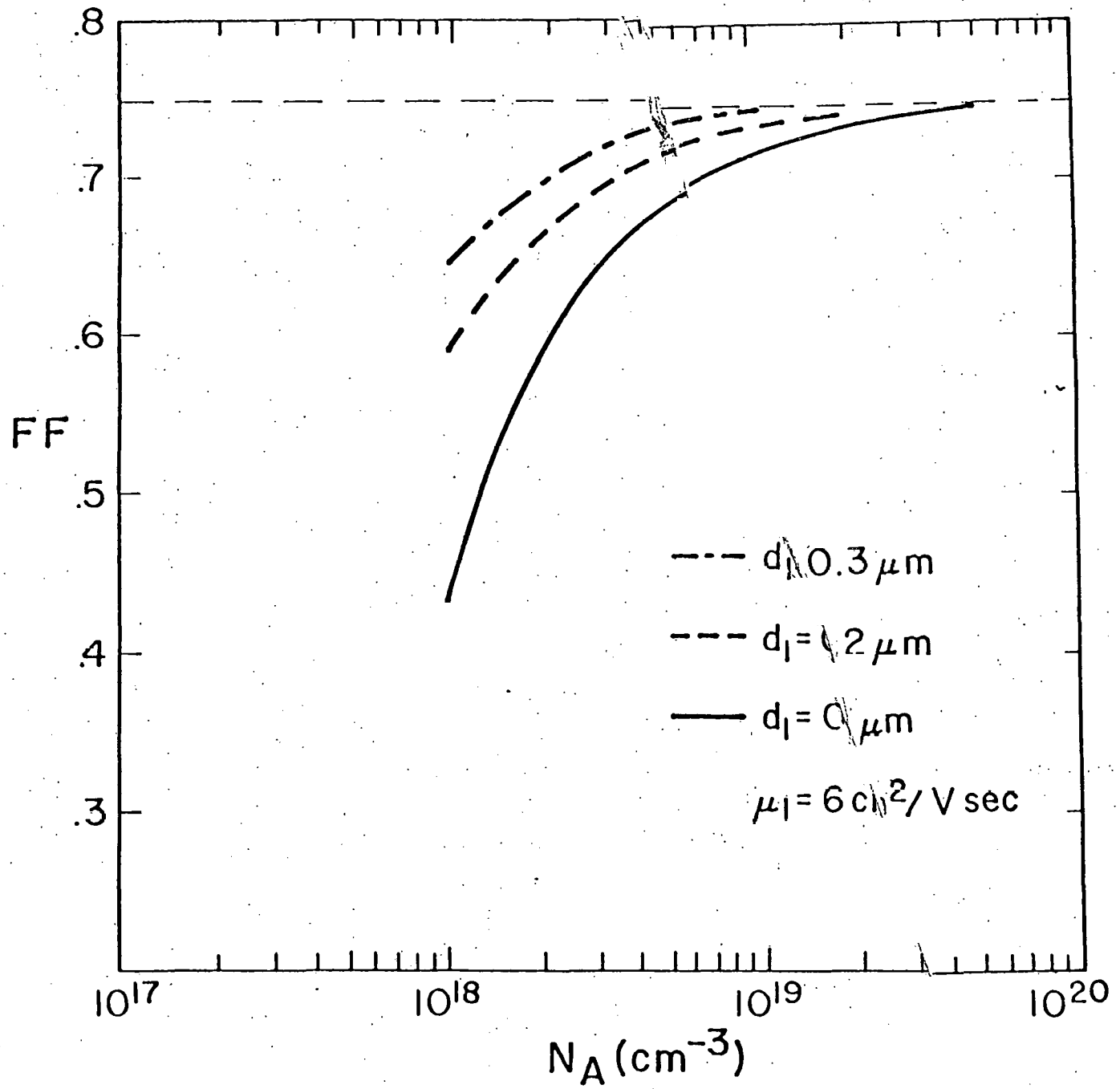
.8
.7
.6
.5
.4
.3
FF
d_1 0.3 μm
d_1 = 0.2 μm
d_1 = 0 μm
μ_1 = 6 cm²/ V sec
10^{17}
10^{18}
10^{19}
10^{20}
N_A (cm^{-3})

Fig. 3

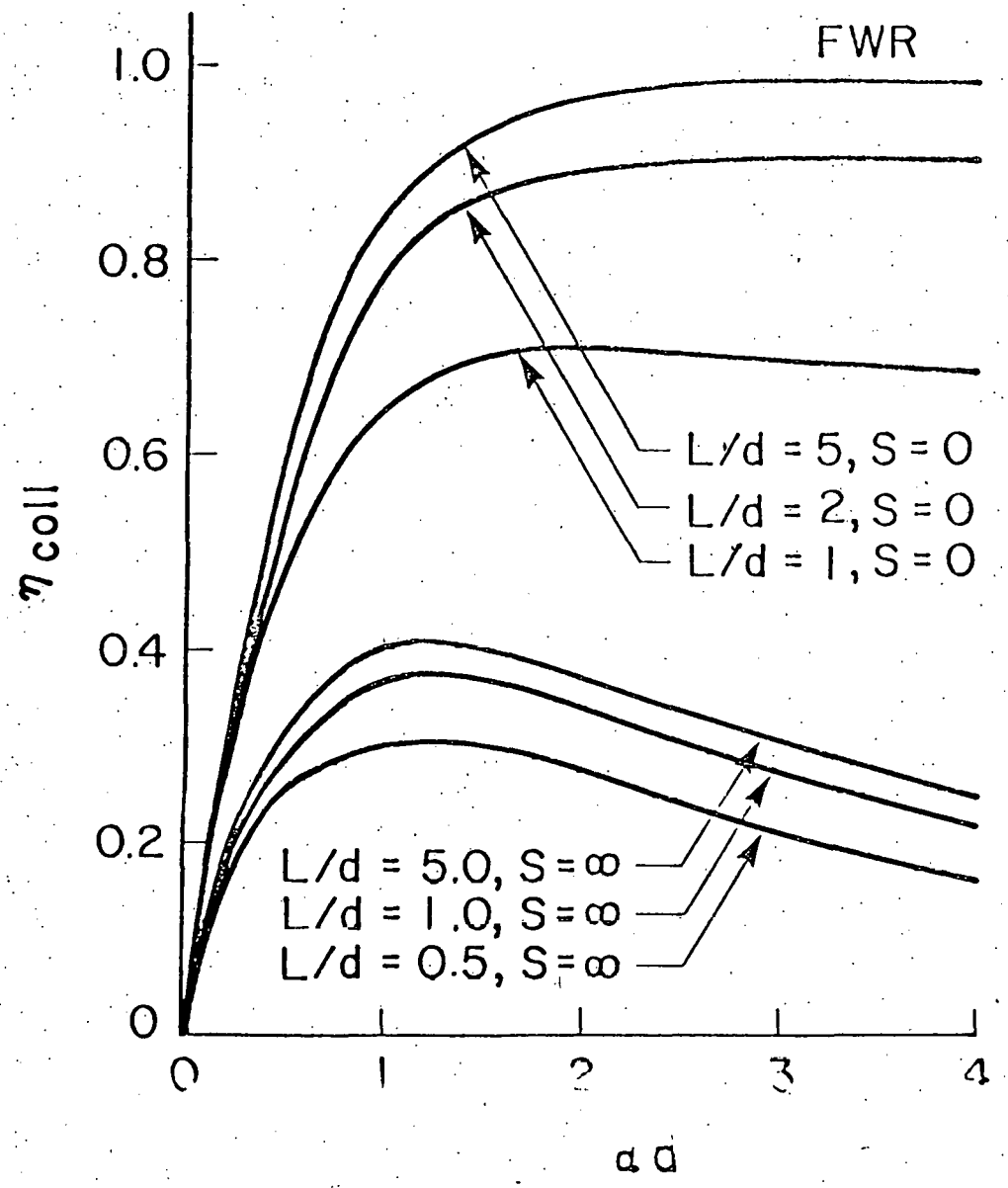
FWR
1.0
0.8
0.6
0.4
0.2
0
η_{coll}
L/d = 5, S = 0
L/d = 2, S = 0
L/d = 1, S = 0
L/d = 5.0, S = ∞
L/d = 1.0, S = ∞
L/d = 0.5, S = ∞
0
1
2
3
4
α d

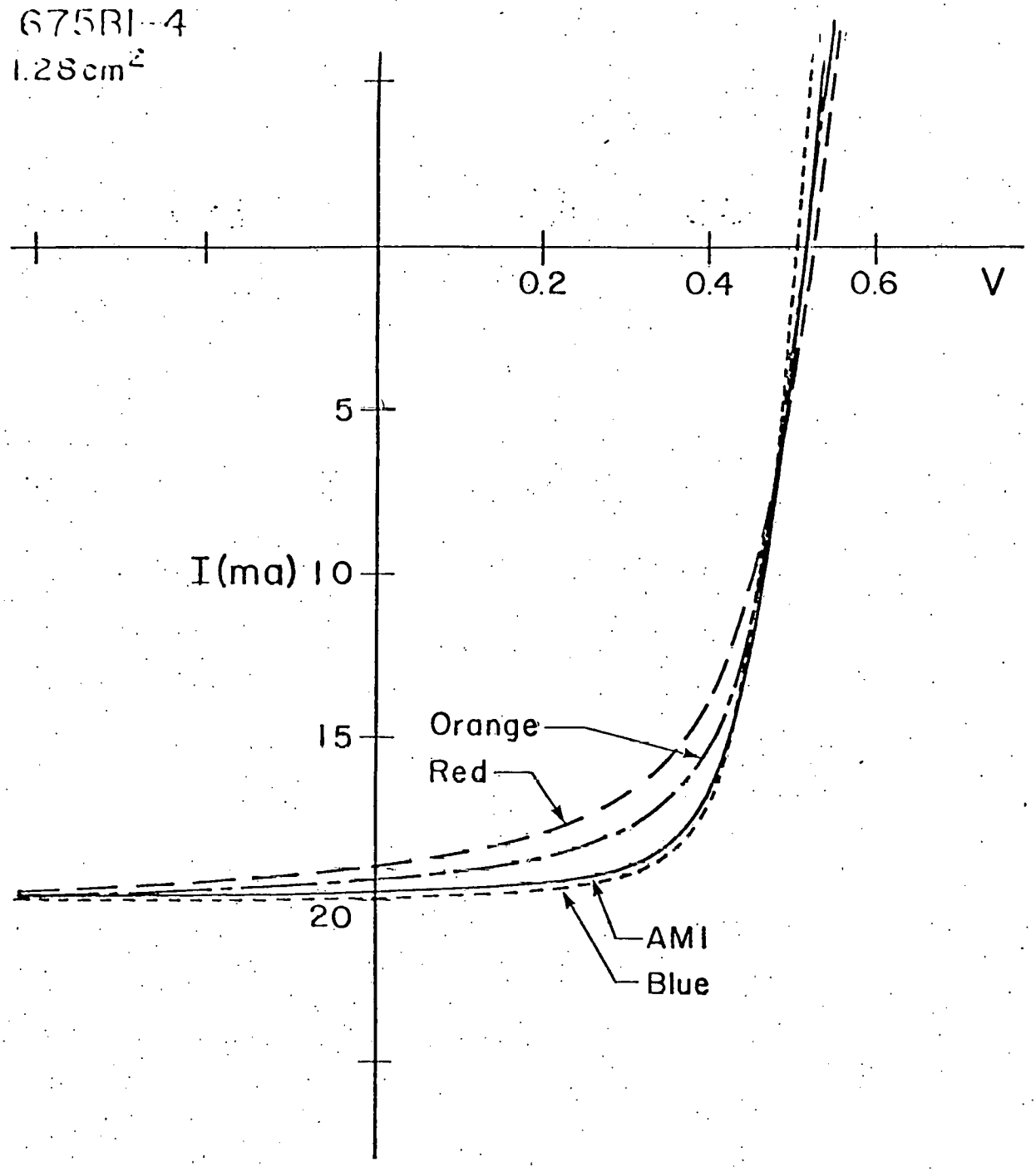
675RI-4
1.28cm²
0.2
0.4
0.6
V
5
I(ma) 10
15
20
Orange
Red
AMI
Blue

Fig. 5

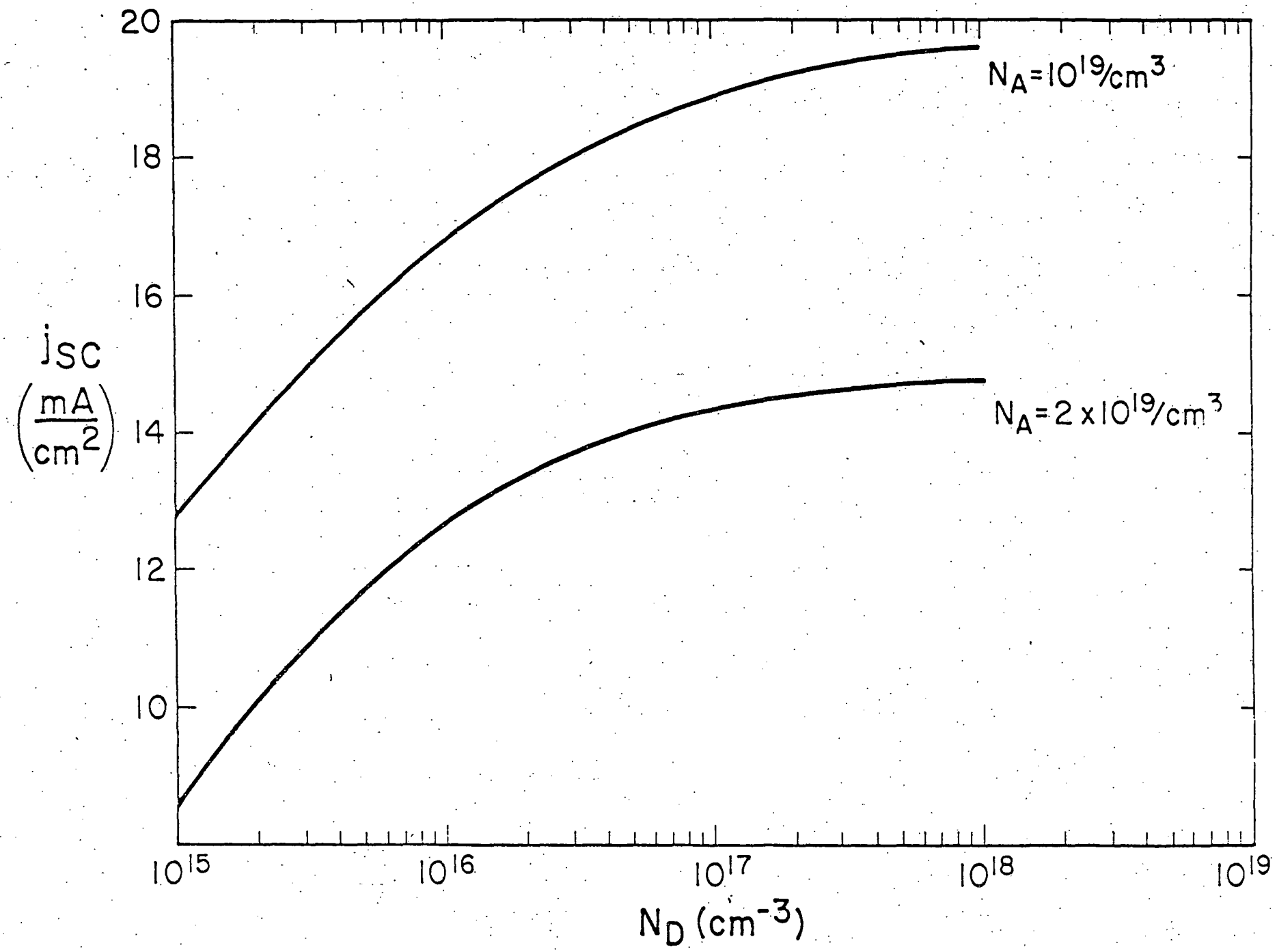
20
18
16
14
12
10
j_{SC}
$\left(\frac{mA}{cm^2}\right)$
$N_A = 10^{19}/cm^3$
$N_A = 2 \times 10^{19}/cm^3$
10^{15}
10^{16}
10^{17}
10^{18}
10^{19}
$N_D\ (cm^{-3})$

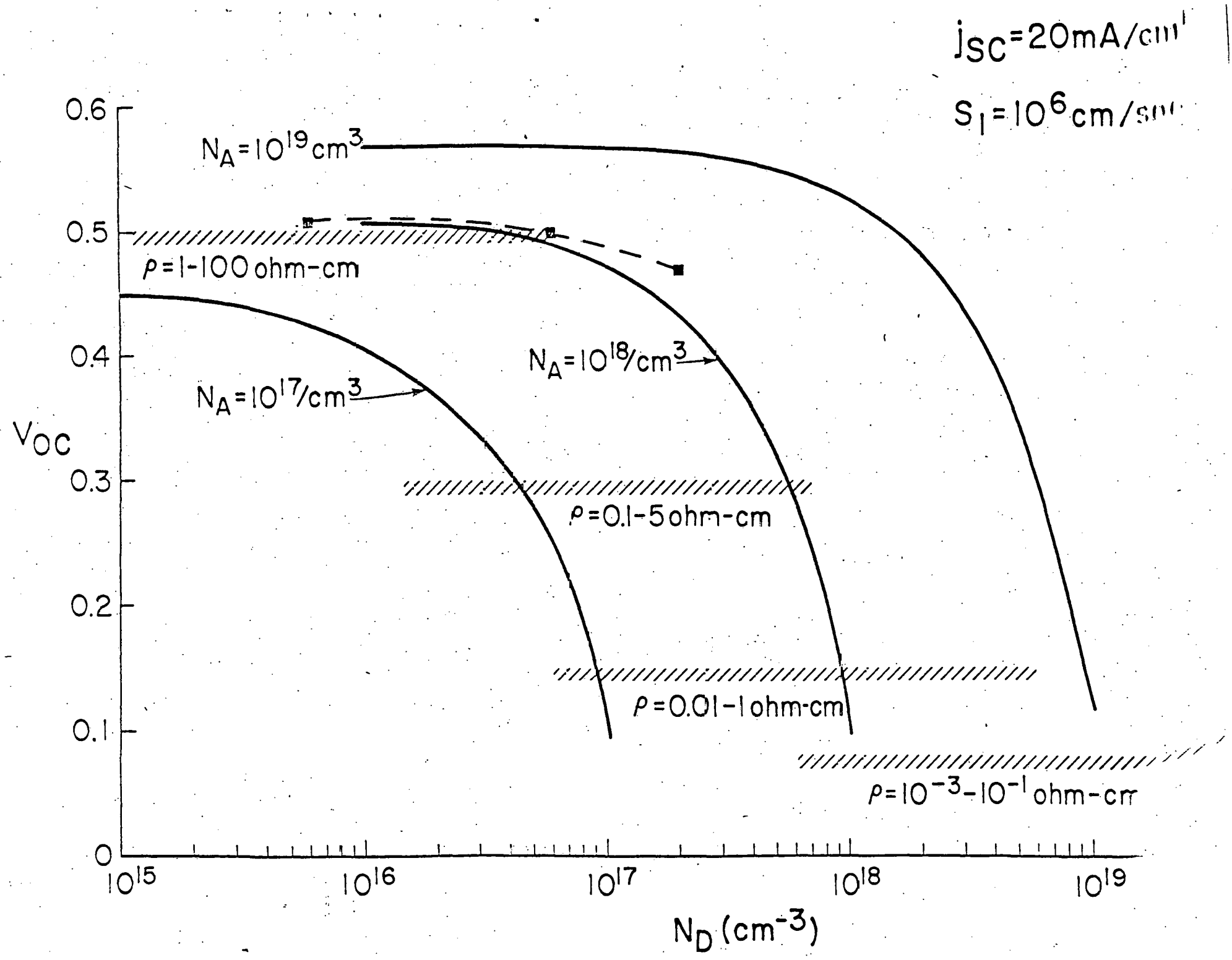
j_{SC}=20mA/cm²
S_1=10⁶cm/sec
N_A=10¹⁹cm⁻³
N_A=10¹⁸/cm³
N_A=10¹⁷/cm³
ρ=1-100 ohm-cm
ρ=0.1-5 ohm-cm
ρ=0.01-1 ohm-cm
ρ=10⁻³-10⁻¹ ohm-cm
V_{OC}
0.6
0.5
0.4
0.3
0.2
0.1
0
10¹⁵
10¹⁶
10¹⁷
10¹⁸
10¹⁹
N_D (cm⁻³)

Fig 7

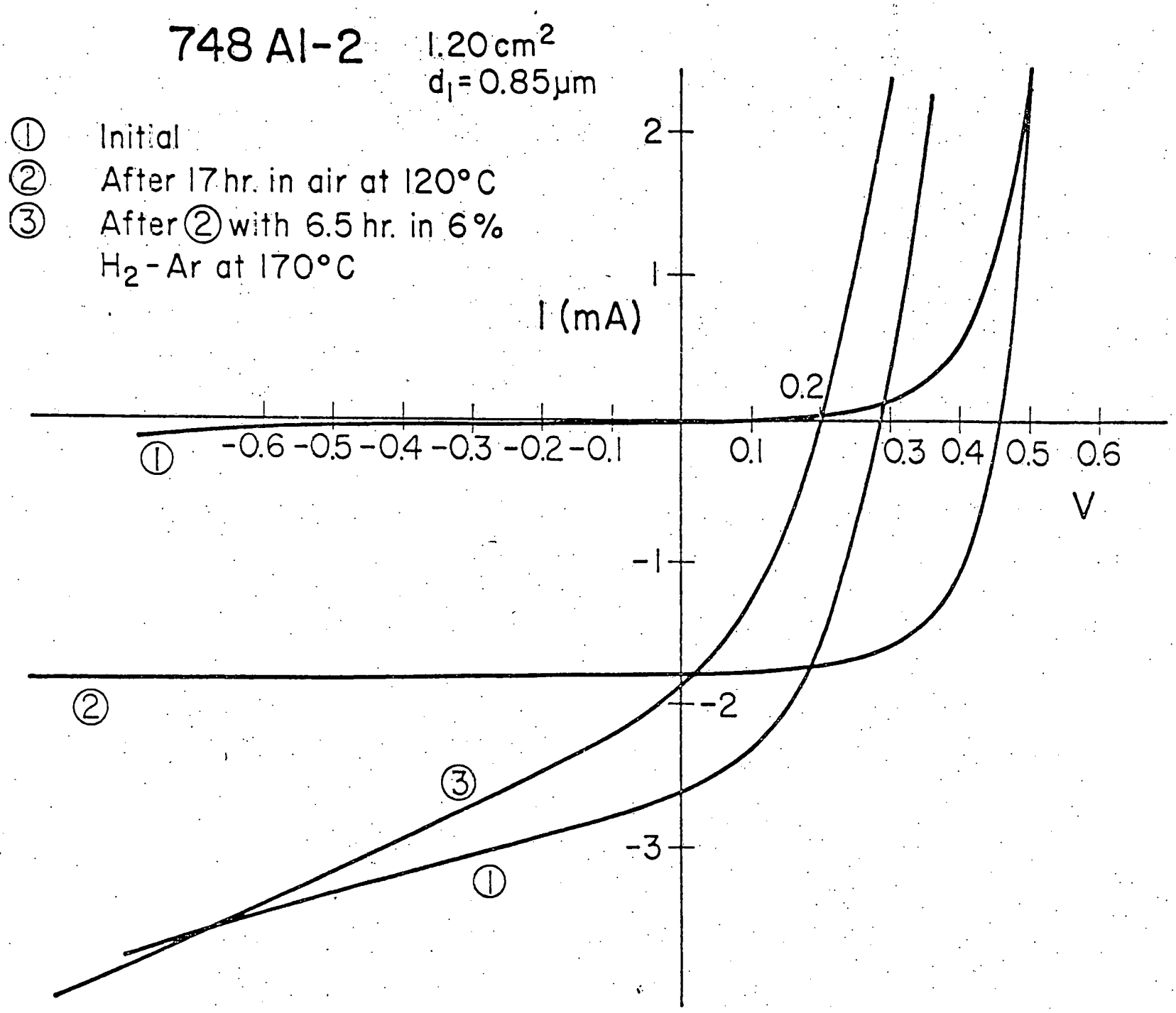
748 Al-2
1.20 cm²
d₁ = 0.85 μm
① Initial
② After 17 hr. in air at 120°C
③ After ② with 6.5 hr. in 6% H₂ - Ar at 170°C
I (mA)
V
2
1
-1
-2
-3
0.2
0.1
0.3
0.4
0.5
0.6
-0.6
-0.5
-0.4
-0.3
-0.2
-0.1
①
②
③